12-2021

Automated Flight Controller Adaptive Compensation for Actuator Failures in Transport Type Aircraft

Daniel James Fresella
University of Arkansas, Fayetteville

Automated Flight Controller Adaptive Compensation for Actuator Failures in Transport Type Aircraft

A thesis submitted in partial fulfillment
of the requirements for the degree of
Master of Science in Electrical Engineering

by

Daniel James Fresella
University of Maryland, College Park
Bachelor of Science in Electrical Engineering, 2016

December 2021
University of Arkansas

This thesis is approved for recommendation to the Graduate Council.

_____
Roy A. McCann, Ph.D.
Thesis Director

_____
Juan Balda, Ph.D.
Committee Member

_____
Jingxian Wu, Ph.D.
Committee Member

Abstract

Aircraft operate over a wide range of conditions including atmospheric, weight, and center of gravity changes. This presents a substantial challenge to automatic control system designers. When these operating conditions are merged with a partial or full control surface failure, automatic flight control is near impossible with conventional controllers. Additionally, when pilots experience control failure emergencies during flight, workload and fatigue increase drastically. The continued research of automatic flight control systems that can seamlessly adapt to unmodelled failures will enable a new generation of robust aircraft control. In this paper a 9^{th} order 6 degree of freedom aircraft model is used to evaluate a transport type aircraft's response to an adaptive controller given unknown actuator failures. A differential thrust transport type aircraft model is developed and modeled in MATLAB and Simulink. A nominal controller is then designed using a linear quadratic regulator (LQR). This generates a model reference response to a perturbed flight condition. An adaptive controller is subsequently implemented as a controller to the linearized aircraft model. This enables the study of convergence to the uninhibited reference output after multiple actuator failures.

Acknowledgement

I would like to thank my family and close friends for their unwavering support during my coursework and research. A special thanks to Dr. Roy McCann for advising my research and thesis writing. Your time is greatly appreciated. Additionally, thank you to Dr. Juan Balda and Dr. Jingxian Wu for being members of my committee and taking the time to review my work.

Table of Contents

List of Tables and Figures

Introduction

Automatic flight control systems enable the precise control of high-performance aircraft, reduce pilot fatigue, and increase flight safety. Both military and civil aircraft have experienced a range of flight control failures resulting in fatal outcomes. It is common for pilots who maintain initial stability of the aircraft to determine alternate means of control. Even after alternative control is achieved, unmodeled dynamics make a safe recovery very difficult if not impossible.

Civil aircraft flight history is filled with aircraft that have suffered actuator failure either through bird strikes or hydraulic system loss. Both emergencies can result in partial or total loss of flight control and the inability to use automatic flight control systems entirely. This rapidly increases pilot workload and maximizes chances of inducing a secondary emergency due to pilot error.

Military aircraft compound the risk of civil aircraft flight. Military aircraft are often flown with increased demand on aircraft systems. In addition to systemic risk, military aircraft are subject to system damage through combat operations and high intensity tactical flying. Damage to flight control surfaces caused by any of the aforementioned reasons has led to loss of aircraft and loss of life.

Previous research has shown that conventional transport type aircraft are controllable through engine thrust alone and are able to inherently stabilize over a wide range of damage and failure patterns [1]. The study of adaptive controllers that can reconfigure to overcome control surface failure or damage can allow a damaged aircraft full or partial controllability; sometimes, even allowing pilots to make safe or survivable landings.

In this thesis a two-engine differential thrust aircraft is modeled in MATLAB and Simulink and subsequently linearized to study its trimmed steady state flight dynamics. The paper will describe the process of modeling an aircraft with the six degrees of freedom equations. It will follow with the linearization of the aircraft using small perturbation theory. The linearized aircraft trimmed at a steady state airspeed, altitude, and attitude will then be used to construct a nominal and adaptive controller.

The nominal controller designed using LTI (Linear Time Invariant) techniques utilizes LQR control with weighted cost function matrices. This achieves desired nominal performance. The outputs from the linearized plant and nominal controller are used as a model reference when evaluating plant state error. The adaptive controller is implemented using adaptive laws known as the "MIT rule" to achieve convergence to the reference output. The adaptive controller in this simulation can achieve convergence without any form of error detection. While this negates the need for cumbersome error detection systems it does result in undesirable control effects before the adaptive gain allows the controller to converge to the nominal response.

A Simulink simulation is used to evaluate the open loop stability dynamics of the model, study nominal controller response, and evaluate adaptive controller learning rates. In Chapter 5 the outcomes of different cost function weightings and learning rates are displayed to evaluate the most desirable flight responses and draw conclusions related to real world implementation.

Chapter 1

Engine Differential Aircraft Modeling

In this chapter a linearized 6-degree of freedom aircraft model is developed for control and simulation. Usually, linearized aircraft models assume symmetric thrust from the left and right engines. It is necessary in this analysis to decouple the left engine, left aileron, right engine, and right aileron. This allows the system's controllers to respond adequately to a set of partial or full flight control surface failures. [2]

To simplify aircraft analysis and simulation, aircraft longitudinal and lateral motion equations are often decoupled. In this paper the longitudinal and lateral equations remain dependent to model the full effects of engine differential thrust.[2]

Below a non-linear aircraft model with differential engine thrust will be derived. This is followed by linearization of the nonlinear model around an equilibrium point using small perturbation theory. The linearized model is numerically solved in [3] to provide a trimmed model of a transport type aircraft in unaccelerated cruise flight.

Aircraft motion is represented by a set of variables and axes. Figure 1-1 displays the variables of motion and force used to characterize the system. Table 1-1 lists their descriptions.

When modeling aircraft there are 3 axes that are used to derive the 6-DOF equations. The 3 axes are the body axes, stability axes, and wind axes. All variables and equations will be rotated to the body axis before linearization using the methods described here.

1.1 Aircraft Reference Frames

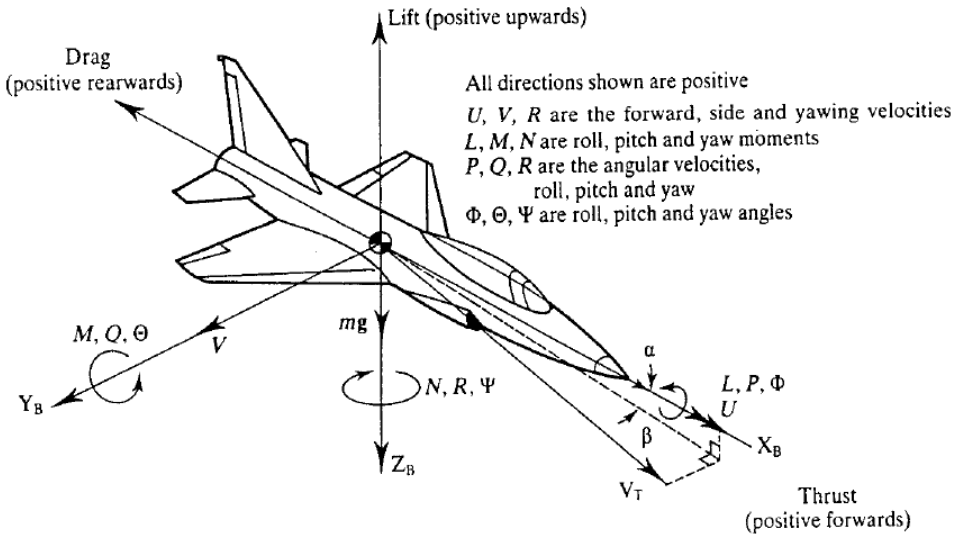

Figure 1-1. Definition of aircraft body axes, velocities, forces, moments, and Euler angles [4].

Table 1-1. Variable Definitions

U	longitudinal (forward) velocity
V	lateral (transverse) velocity
W	vertical velocity
P	roll rate
Q	pitch rate
R	yaw rate
ϕ	roll angle
θ	pitch angle
Ψ	yaw angle
X	longitudinal force
Y	transverse force
Z	vertical force
L	roll moment
M	pitch moment
N	yaw moment

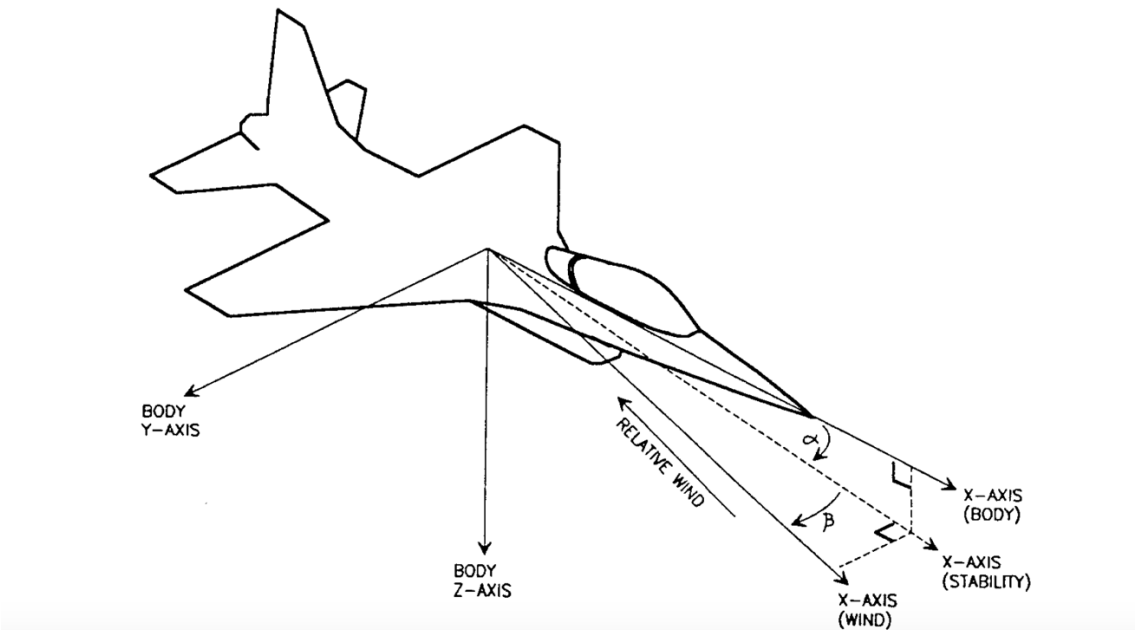

Figure 1-2. Definition of stability and wind axes for an aircraft.[5]

The axes depicted in Figure 1-3 are defined using the angle of attack (α) and sideslip angel (β). These variables are defined mathematically in equations 1.1-1.3.

$$tan(\alpha) = \frac{W}{U} \tag{1.1}$$

$$sin(\beta) = \frac{V}{V_T} \tag{1.2}$$

$$V_T = \sqrt{U^2 + V^2 + W^2} \tag{1.3}$$

1.2 Euler Rotation Matrices

Rotation matrices are used to rotate values derived in different reference frames to the desired reference frame. In this case we need to rotate all equations into the body axes to develop the non-linear model. The rotation matrices below defined in [5] represent the relationships between each coordinate system or reference frame.

$$R_b^s = \begin{bmatrix} cos(\alpha) & 0 & sin(\alpha) \\ 0 & 1 & 0 \\ -sin(\alpha) & 0 & cos(\alpha) \end{bmatrix} \tag{1.4}$$

$$R_s^w = \begin{bmatrix} cos(\beta) & sin(\beta) & 0 \\ -sin(\beta) & cos(\beta) & 0 \\ 0 & 0 & 1 \end{bmatrix} \tag{1.5}$$

$$R_b^w = R_b^s * R_s^w = \begin{bmatrix} cos(\alpha)cos(\beta) & sin(\beta) & sin(\alpha)cos(\beta) \\ -cos(\alpha)sin(\beta) & cos(\beta) & -sin(\alpha)sin(\beta) \\ -sin(\alpha) & 0 & cos(\alpha) \end{bmatrix} \tag{1.6}$$

$$R_{z,\Psi} = R_s^w \ \ Where \ \Psi \cong \beta \tag{1.7}$$

$$R_{y,\theta} = R_s^w \ Where \ \theta \cong \alpha \tag{1.8}$$

$$R_{x,\phi} = \begin{bmatrix} 1 & 0 & 0 \\ 0 & cos(\phi) & -sin(\phi) \\ 0 & sin(\phi) & cos(\phi) \end{bmatrix} \tag{1.9}$$

1.3 Euler Angle Kinematics

$$\begin{bmatrix} P \\ Q \\ R \end{bmatrix} = \begin{bmatrix} \dot{\phi} \\ 0 \\ 0 \end{bmatrix} + R_{x,\phi}^T \begin{bmatrix} 0 \\ \dot{\theta} \\ 0 \end{bmatrix} + R_{x,\phi}^T R_{y,\theta}^T \begin{bmatrix} 0 \\ 0 \\ \dot{\Psi} \end{bmatrix} \tag{1.10}$$

$$\begin{bmatrix} \dot{\phi} \\ \dot{\theta} \\ \dot{\Psi} \end{bmatrix} = \begin{bmatrix} 1 & sin(\phi)tan(\theta) & cos(\phi)tan(\theta) \\ 0 & cos(\phi) & -sin(\phi) \\ 0 & sin(\phi)/cos(\theta) & cos(\phi)/cos(\theta) \end{bmatrix} \begin{bmatrix} P \\ Q \\ R \end{bmatrix} \tag{1.11}$$

$$\dot{\phi} = p + tan(\theta))(Qsin(\phi) + Rcos(\phi)) \tag{1.12}$$

$$\dot{\theta} = Qcos(\phi) - Rsin(\phi) \tag{1.13}$$

$$\dot{\psi} = \frac{Qsin(\phi) + Rcos(\phi)}{cos(\theta)} \tag{1.14}$$

1.4 Rigid-body Kinetics

$$I_{CG} = \begin{bmatrix} I_x & 0 & -I_{xz} \\ 0 & I_y & 0 \\ -I_{xz} & 0 & I_z \end{bmatrix} \tag{1.15}$$

$$m\left(\begin{bmatrix}\dot{U}\\ \dot{V}\\ \dot{W}\end{bmatrix}+\begin{bmatrix}P\\ Q\\ R\end{bmatrix}\times\begin{bmatrix}U\\ V\\ W\end{bmatrix}\right)=\begin{bmatrix}X\\ Y\\ Z\end{bmatrix} \tag{1.16}$$

where, $\times$ denotes vector cross product

$$I_{CG}\begin{bmatrix}\dot{P}\\ \dot{Q}\\ \dot{R}\end{bmatrix}+\begin{bmatrix}P\\ Q\\ R\end{bmatrix}\times I_{CG}\begin{bmatrix}P\\ Q\\ R\end{bmatrix})=\begin{bmatrix}L\\ M\\ N\end{bmatrix} \tag{1.17}$$

$$S_1=\begin{bmatrix}0 & -R & Q\\ R & 0 & -P\\ -Q & P & 0\end{bmatrix} \tag{1.18}$$

$$S_2=\begin{bmatrix}0 & I_{xz}-I_zR & I_yQ\\ -I_{xz}P+I_zR & 0 & -I_xP+I_{xy}R\\ -I_yQ & I_xP-I_{xy}R & 0\end{bmatrix} \tag{1.19}$$

$$M=\begin{bmatrix}mI_{3x3} & 0_{3x3}\\ 0_{3x3} & I_{cg}\end{bmatrix} \tag{1.20}$$

$$C=\begin{bmatrix}mS_1 & 0_{3x3}\\ 0_{3x3} & -S_2\end{bmatrix} \tag{1.21}$$

$$G=\begin{bmatrix}mg\ sin(\theta)\\ -mg\ cos(\theta)sin(\phi)\\ -mg\ cos(\theta)\ cos(\phi)\\ 0\\ 0\\ 0\end{bmatrix} \tag{1.22}$$

$$M\begin{bmatrix}\dot{U}\\ \dot{V}\\ \dot{W}\\ \dot{P}\\ \dot{Q}\\ \dot{R}\end{bmatrix}+C\begin{bmatrix}U\\ V\\ W\\ P\\ Q\\ R\end{bmatrix}+G=\begin{bmatrix}X\\ Y\\ Z\\ L\\ M\\ N\end{bmatrix} \tag{1.23}$$

1.5 Non-Linear Aircraft Equations

Using rigid body dynamics equations and an Inertia tensor representing XZ-plane symmetry defined in [4], [5] a generalized set of nonlinear rigid body equations of motion can be derived.

$$m(\dot{U} + QW - RV + gsin(\theta)) = X \quad (1.24)$$

$$m(\dot{V} + UR - WP - gcos(\theta)sin(\phi)) = Y \quad (1.25)$$

$$m(\dot{W} + VP - QU + gcos(\theta)cos(\phi)) = Z \quad (1.26)$$

$$I_x\dot{P} - I_{xz}(\dot{R} + PQ) + (I_z - I_y)QR = L \quad (1.27)$$

$$I_y\dot{Q} + I_{xz}(P^2 - R^2) + (I_x - I_z)PR = M \quad (1.28)$$

$$I_z\dot{R} - I_{xz}\dot{P} + (I_y - I_x)PQ + I_{xz}QR = N \quad (1.29)$$

1.6 Differential Thrust Modeling

$$m(\dot{U} + QW - RV) = X - mgsin(\theta) + (T_L + T_R)cos(\epsilon) \quad (1.30)$$

$$m(\dot{V} + UR - WP) = Y + mgcos(\theta)sin(\phi) \quad (1.31)$$

$$m(\dot{W} + VP - QU) = Z + mgcos(\theta)cos(\phi) - (T_L + T_R)sin(\epsilon) \quad (1.32)$$

$$I_x\dot{P} - I_{xz}(\dot{R} + PQ) + (I_z - I_y)QR = L + \ell(T_L + T_R)sin(\epsilon) \quad (1.33)$$

$$I_y\dot{Q} + I_{xz}(P^2 - R^2) + (I_x - I_z)PR = M \quad (1.34)$$

$$I_z\dot{R} - I_{xz}\dot{P} + (I_y - I_x)PQ + I_{xz}QR = N + \ell(T_L + T_R)cos(\epsilon) \quad (1.35)$$

Where T_L = left engine force, T_R = right engine force, and ℓ = distance between body x-axis. Figures 1-4 through 1-6 depict the engine centerline displacement and the variable "ϵ." "ϵ" represents the angle the engines are mounted with respect to the longitudinal and lateral plane.

1.7 Aircraft Model Linearization

The nonlinear rigid body and attitude equations derived in sections 1.1 – 1.6 can be linearized using small perturbation theory. In this section we will generally linearize the 6-DOF (degrees of freedom) equations around an unspecified equilibrium point. Later in this section the equilibrium

point will be defined in reference to [2]. The next section will outline the numerical model used for simulation based on the small perturbation linearization and the trimmed flight condition.

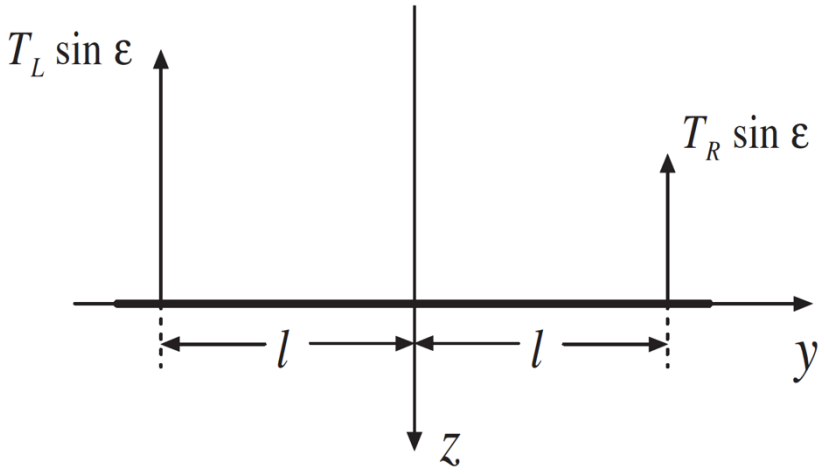

Figure 1-3. Engine thrust components in the y–z plane. [2]

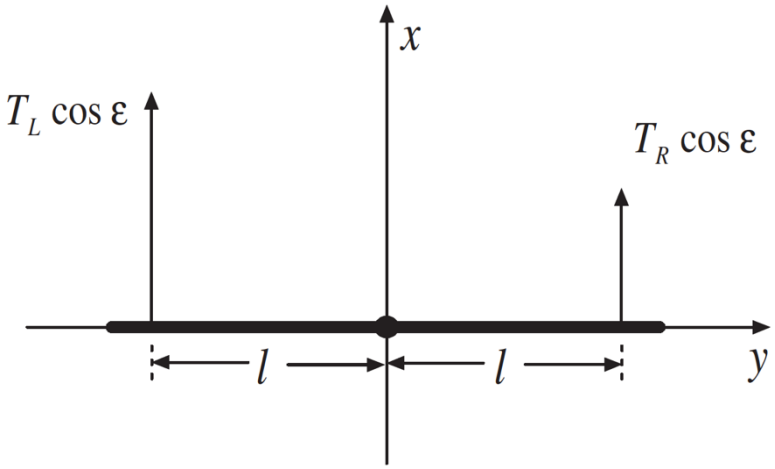

Figure 1-4. Engine thrust components in the x–y plane. [2]

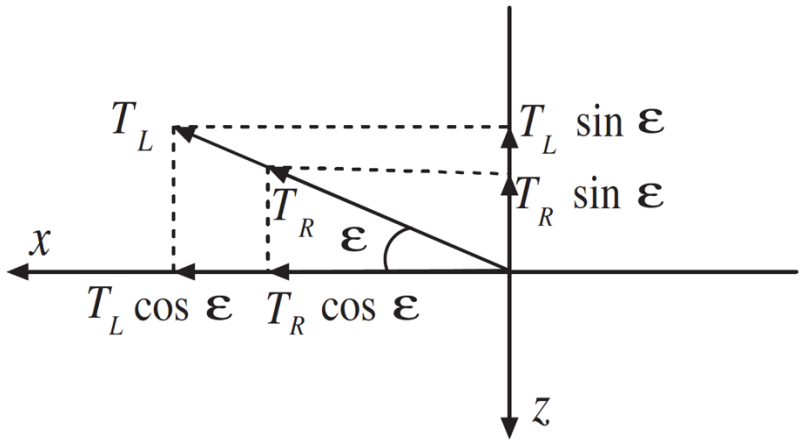

Figure 1-5. Engine thrust components in the x–z plane. [2]

For linearization all aerodynamic forces, moments, velocities, angles, and control inputs will be expressed as nominal values in addition to their perturbations. The perturbation values are denoted with "δ."

$$x = x_o + \delta x \; and \; u = u_o + \delta u \tag{1.36}$$

Where *x* denotes the state vector and *u* denoted the control vector. To perform the linearization. The state space variables are explicitly defined and subsequently linearized using small perturbation theory and small angle assumptions.

$$x = [u \quad w \quad q \quad \theta \quad v \quad r \quad p \quad \phi \quad \psi]^T \tag{1.37}$$

$$u = [\delta_e \quad \delta_{t_l} \quad \delta_{t_r} \quad \delta_{a_l} \quad \delta_{a_r} \quad \delta_r]^T \tag{1.38}$$

$$[\dot{u} \quad \dot{w} \quad \dot{q} \quad \dot{\theta} \quad \dot{v} \quad \dot{r} \quad \dot{p} \quad \dot{\phi} \quad \dot{\psi}]_{x_o,U_o} = 0 \tag{1.39}$$

$$p_o = q_o = r_o = \phi_o = \psi_o = v_o = 0 \tag{1.40}$$

$$x_o = [u_o \quad w_o \quad 0 \quad \theta_o \quad 0 \quad 0 \quad 0 \quad 0 \quad 0]^T \tag{1.41}$$

$$u_o = [\delta_{eo} \quad \delta_{t_l o} \quad \delta_{t_r o} \quad \delta_{a_l o} \quad \delta_{a_r o} \quad \delta_{ro}]^T \tag{1.42}$$

Force Equations,

$$\dot{u} = \frac{1}{m}X - g\,sin(\theta) + \frac{1}{m}(T_L + T_R)cos(\epsilon) - qw + rv \tag{1.43}$$

$$\dot{v} = \frac{1}{m}Y + g\,cos(\theta)sin(\phi) - ru + pw \tag{1.44}$$

$$\dot{w} = \frac{1}{m}Z + g\,cos(\theta)cos(\phi) + \frac{1}{m}(T_L + T_R)sin(\epsilon) - pv + qu \tag{1.45}$$

Moment Equations,

$$\dot{p} = c_1 qr + c_2 qp + c_3 L - c_4 N + c_5 \ell (T_L + T_R) \tag{1.46}$$

$$\dot{q} = c_1 qr + c_2 qp + c_3 L - c_4 N + c_5 \ell (T_L + T_R) \tag{1.47}$$

$$\dot{r} = c_9 q - c_2 qr + c_{10} N - c_{11} L + c_{12} \ell (T_L + T_R) \tag{1.48}$$

Where, c_i is defined in [2] and Figure 1-7.

$$c_1 = \frac{I_y I_z - I_{xy}^2 - I_z^2}{I_x I_z - I_{xz}^2}, \quad c_2 = \frac{I_{xz} I_y - I_z I_{xz} - I_x I_{xz}}{I_x I_z - I_{xz}^2},$$
$$c_3 = \frac{I_z}{I_x I_z - I_{xz}^2}, \quad c_4 = \frac{I_{xz}}{I_x I_z - I_{xz}^2},$$
$$c_5 = \frac{I_z \sin\epsilon - I_{xz}\cos\epsilon}{I_x I_z - I_{xz}^2}, \quad c_6 = \frac{I_z - I_x}{I_y},$$
$$c_7 = \frac{I_{xz}}{I_y}, \quad c_8 = \frac{1}{I_y},$$
$$c_9 = \frac{I_x^2 + I_{xz}^2 - I_x I_y}{I_x I_z - I_{xz}^2}, \quad c_{10} = \frac{I_x}{I_x I_z - I_{xz}^2},$$
$$c_{11} = \frac{I_{xz}}{I_x I_z - I_{xz}^2}, \quad c_{12} = \frac{I_x \cos\epsilon - I_{xz}\sin\epsilon}{I_x I_z - I_{xz}^2}.$$

Figure 1-7. Moment equation constants [2]

Attitude Equations,

$$\dot{\phi} = p + tan(\theta))(Qsin(\phi) + Rcos(\phi))$$

(1.49)

$$\dot{\theta} = Qcos(\phi) - Rsin(\phi) \quad (1.50)$$

$$\dot{\psi} = \frac{Qsin(\phi) + Rcos(\phi)}{cos(\theta)} \quad (1.51)$$

Finally, the longitudinal and lateral moments are added to the right side of the force and moment equations as in [4]. The force and moment derivative notation is described in Figure 1-8. The equations are then linearized using a small angle approximation and small perturbation theory as in [4]. The resulting aircraft model is outlined in the next section.

$$X_{\text{index}} = \frac{\partial X}{\partial \text{ index}} \quad L_{\text{index}} = \frac{\partial L}{\partial \text{ index}}$$
$$Y_{\text{index}} = \frac{\partial Y}{\partial \text{ index}} \quad M_{\text{index}} = \frac{\partial M}{\partial \text{ index}}$$
$$Z_{\text{index}} = \frac{\partial Z}{\partial \text{ index}} \quad N_{\text{index}} = \frac{\partial N}{\partial \text{ index}}$$

Figure 1-8. Force and moment derivative notation [4]

1.8 Linearized Aircraft Model

The airplane flies at a velocity of 774 ft/sec (458.6 knots) and an altitude of 40 thousand feet. The linearized dynamic model is below. The basic units used in this model are ft, sec and crad (0.01 radian). Later in the paper the results will be displayed in terms of degrees using a crad to degree conversion factor of 0.572958. Degrees are the units of choice when intuitively determining aircraft attitude [2].

$$\dot{x}(t) = \begin{bmatrix} A^{(1)}_{4\times4} & A^{(2)}_{4\times5} \\ A^{(3)}_{5\times4} & A^{(4)}_{5\times5} \end{bmatrix} x(t) + \begin{bmatrix} B^{(1)}_{4\times3} & B^{(2)}_{4\times3} \\ B^{(3)}_{5\times3} & B^{(4)}_{5\times3} \end{bmatrix} U(t),$$

Figure 1-8-1. Linearized state space model [2].

The state space model and supporting matrices and derivatives are shown in Figures 1-8-1, 1-9, 1-10, and 1-11.

$$A^{(1)} = \begin{bmatrix} \bar{X}_u & \bar{X}_w & -w_o & -g\cos\theta_o \\ \bar{Z}_u & \bar{Z}_w & u_o & -g\sin\theta_o \\ \bar{M}_u & \bar{M}_w & \bar{M}_q & 0 \\ 0 & 0 & 1 & 0 \end{bmatrix}, \quad B^{(1)} = \begin{bmatrix} X_{\delta_e} & \bar{T}_{\delta_{t_l}} & \bar{T}_{\delta_{t_r}} \\ Z_{\delta_e} & -\bar{T}'_{\delta_{t_l}} & -\bar{T}'_{\delta_{t_r}} \\ \bar{M}_{\delta_e} & 0 & 0 \\ 0 & 0 & 0 \end{bmatrix},$$

$$A^{(2)} = \begin{bmatrix} 0 & 0 & 0 & 0 & 0 \\ 0 & 0 & 0 & 0 & 0 \\ 0 & 0 & 0 & 0 & 0 \\ 0 & 0 & 0 & 0 & 0 \end{bmatrix}, \quad B^{(2)} = \begin{bmatrix} 0 & 0 & 0 \\ 0 & 0 & 0 \\ 0 & 0 & 0 \\ 0 & 0 & 0 \end{bmatrix},$$

$$A^{(3)} = \begin{bmatrix} 0 & 0 & 0 & 0 \\ \bar{T}_u & \bar{T}_w & 0 & 0 \\ \bar{T}'_u & \bar{T}'_w & 0 & 0 \\ 0 & 0 & 0 & 0 \\ 0 & 0 & 0 & 0 \end{bmatrix}, \quad B^{(3)} = \begin{bmatrix} 0 & 0 & 0 \\ 0 & \bar{T}''_{\delta_{t_l}} & -\bar{T}''_{\delta_{t_r}} \\ 0 & \bar{T}'''_{\delta_{t_l}} & -\bar{T}'''_{\delta_{t_r}} \\ 0 & 0 & 0 \\ 0 & 0 & 0 \end{bmatrix},$$

$$A^{(4)} = \begin{bmatrix} Y_v & -u_o & w_o & g\cos\theta_o & 0 \\ \bar{N}_v & \bar{N}_r & \bar{N}_p & 0 & 0 \\ \bar{L}_v & \bar{L}_r & \bar{L}_p & 0 & 0 \\ 0 & \tan\theta_o & 1 & 0 & 0 \\ 0 & \frac{1}{\cos\theta_o} & 0 & 0 & 0 \end{bmatrix} \quad B^{(4)} = \begin{bmatrix} Y_{\delta_{al}} & Y_{\delta_{ar}} & Y_{\delta_r} \\ \bar{N}_{\delta_{al}} & \bar{N}_{\delta_{ar}} & \bar{N}_{\delta_r} \\ \bar{L}_{\delta_{al}} & \bar{L}_{\delta_{ar}} & \bar{L}_{\delta_r} \\ 0 & 0 & 0 \\ 0 & 0 & 0 \end{bmatrix}.$$

Figure 1-9. A and B state space symbolic matrices [2].

$$
\begin{aligned}
\bar{X}_u &= \tfrac{1}{m}[\tfrac{\partial X}{\partial u} + \cos\epsilon(\tfrac{\partial T_L}{\partial u} + \tfrac{\partial T_R}{\partial u})], \\
\bar{X}_w &= \tfrac{1}{m}[\tfrac{\partial X}{\partial w} + \cos\epsilon(\tfrac{\partial T_L}{\partial w} + \tfrac{\partial T_R}{\partial w})], \\
\bar{Z}_u &= \tfrac{1}{m}[\tfrac{\partial Z}{\partial u} - \sin\epsilon(\tfrac{\partial T_L}{\partial u} + \tfrac{\partial T_R}{\partial u})], \\
\bar{Z}_w &= \tfrac{1}{m}[\tfrac{\partial Z}{\partial w} - \sin\epsilon(\tfrac{\partial T_L}{\partial w} + \tfrac{\partial T_R}{\partial w})],
\end{aligned}
$$

$$
\begin{aligned}
\bar{M}_u &= c_8(\tfrac{\partial M}{\partial u}), & \bar{M}_w &= c_8(\tfrac{\partial M}{\partial w}), \\
\bar{M}_q &= c_8(\tfrac{\partial M}{\partial q}), & \bar{T}_u &= c_{12}l(\tfrac{\partial T_L}{\partial u} - \tfrac{\partial T_R}{\partial u}), \\
\bar{T}_w &= c_{12}l(\tfrac{\partial T_L}{\partial w} - \tfrac{\partial T_R}{\partial w}), & \bar{T}'_u &= c_5 l(\tfrac{\partial T_L}{\partial u} - \tfrac{\partial T_R}{\partial u}), \\
\bar{T}'_w &= c_5 l(\tfrac{\partial T_L}{\partial w} - \tfrac{\partial T_R}{\partial w}), & Y_v &= \tfrac{1}{m}\tfrac{\partial Y}{\partial v}, \\
\bar{N}_v &= c_{10}\tfrac{\partial N}{\partial v} - c_{11}\tfrac{\partial L}{\partial v}, & \bar{N}_r &= c_{10}\tfrac{\partial N}{\partial r} - c_{11}\tfrac{\partial L}{\partial r}, \\
\bar{N}_p &= c_{10}\tfrac{\partial N}{\partial p} - c_{11}\tfrac{\partial L}{\partial p}, & \bar{L}_v &= c_3\tfrac{\partial L}{\partial v} - c_4\tfrac{\partial N}{\partial v},
\end{aligned}
$$

$$
\begin{aligned}
\bar{L}_r &= c_3\tfrac{\partial L}{\partial r} - c_4\tfrac{\partial N}{\partial r}, & \bar{L}_p &= c_3\tfrac{\partial L}{\partial p} - c_4\tfrac{\partial N}{\partial p}, \\
X_{\delta_e} &= \tfrac{1}{m}(\tfrac{\partial X}{\partial \delta_e}), & \bar{T}_{\delta_{t_l}} &= \tfrac{\cos\epsilon}{m}(\tfrac{\partial T_L}{\partial \delta_{t_l}}), \\
\bar{T}_{\delta_{t_r}} &= \tfrac{\cos\epsilon}{m}(\tfrac{\partial T_R}{\partial \delta_{t_r}}), & Z_{\delta_e} &= \tfrac{1}{m}(\tfrac{\partial Z}{\partial \delta_e}), \\
\bar{T}'_{\delta_{t_l}} &= \tfrac{\sin\epsilon}{m}(\tfrac{\partial T_L}{\partial \delta_{t_l}}), & \bar{T}'_{\delta_{t_r}} &= \tfrac{\sin\epsilon}{m}(\tfrac{\partial T_R}{\partial \delta_{t_r}}), \\
\bar{M}_{\delta_e} &= c_8\tfrac{\partial M}{\partial \delta_e}, & \bar{T}''_{\delta_{t_l}} &= c_{12}l(\tfrac{\partial T_L}{\partial \delta_{t_l}}), \\
\bar{T}''_{\delta_{t_r}} &= c_{12}l(\tfrac{\partial T_R}{\partial \delta_{t_r}}), & \bar{T}'''_{\delta_{t_l}} &= c_5 l(\tfrac{\partial T_L}{\partial \delta_{t_l}}), \\
\bar{T}'''_{\delta_{t_r}} &= c_5 l(\tfrac{\partial T_R}{\partial \delta_{t_r}}), & Y_{\delta_{al}} &= \tfrac{1}{m}(\tfrac{\partial Y}{\partial \delta_{al}}), \\
Y_{\delta_{ar}} &= \tfrac{1}{m}(\tfrac{\partial Y}{\partial \delta_{ar}}), & Y_{\delta_r} &= \tfrac{1}{m}(\tfrac{\partial Y}{\partial \delta_r}), \\
\bar{N}_{\delta_{al}} &= c_{10}\tfrac{\partial N}{\partial \delta_{al}} - c_{11}\tfrac{\partial L}{\partial \delta_{al}}, & \bar{N}_{\delta_{ar}} &= c_{10}\tfrac{\partial N}{\partial \delta_{ar}} - c_{11}\tfrac{\partial L}{\partial \delta_{ar}}, \\
\bar{N}_{\delta_r} &= c_{10}\tfrac{\partial N}{\partial \delta_r} - c_{11}\tfrac{\partial L}{\partial \delta_r}, & \bar{L}_{\delta_{al}} &= c_3\tfrac{\partial L}{\partial \delta_{al}} - c_4\tfrac{\partial N}{\partial \delta_{al}}, \\
\bar{L}_{\delta_{ar}} &= c_3\tfrac{\partial L}{\partial \delta_{ar}} - c_4\tfrac{\partial N}{\partial \delta_{ar}}, & \bar{L}_{\delta_r} &= c_3\tfrac{\partial L}{\partial \delta_r} - c_4\tfrac{\partial N}{\partial \delta_r}.
\end{aligned}
$$

Figure 1-10. Force and moment derivatives [2]

$$
A^{(1)} = \begin{bmatrix} -0.003 & 0.039 & 0 & -0.322 \\ -0.065 & -0.319 & 7.74 & 0 \\ 0.020 & -0.101 & -0.429 & 0 \\ 0 & 0 & 1 & 0 \end{bmatrix}
\qquad
B^{(1)} = \begin{bmatrix} 0.01 & 1 & 1 \\ -0.18 & -0.04 & -0.04 \\ -1.16 & 0.598 & 0.598 \\ 0 & 0 & 0 \end{bmatrix},
$$

$$
A^{(2)} = \begin{bmatrix} 0 & 0 & 0 & 0 & 0 \\ 0 & 0 & 0 & 0 & 0 \\ 0 & 0 & 0 & 0 & 0 \\ 0 & 0 & 0 & 0 & 0 \end{bmatrix},
\qquad
B^{(2)} = \begin{bmatrix} 0 & 0 & 0 \\ 0 & 0 & 0 \\ 0 & 0 & 0 \\ 0 & 0 & 0 \end{bmatrix},
$$

$$
A^{(3)} = \begin{bmatrix} 0 & 0 & 0 & 0 \\ 0.001 & 0.001 & 0 & 0 \\ -0.001 & -0.001 & 0 & 0 \\ 0 & 0 & 0 & 0 \\ 0 & 0 & 0 & 0 \end{bmatrix},
\qquad
B^{(3)} = \begin{bmatrix} 0 & 0 & 0 \\ 0 & 0.8 & -0.7 \\ 0 & -0.5 & 0.6 \\ 0 & 0 & 0 \\ 0 & 0 & 0 \end{bmatrix},
$$

$$
A^{(4)} = \begin{bmatrix} -0.0558 & -7.74 & 0 & 0.322 & 0 \\ 0.0773 & -0.115 & -0.0318 & 0 & 0 \\ -0.394 & 0.388 & -0.465 & 0 & 0 \\ 0 & 0 & 1 & 0 & 0 \\ 0 & 1 & 0 & 0 & 0 \end{bmatrix}
\qquad
B^{(4)} = \begin{bmatrix} 0.03 & -0.03 & 0.0564 \\ 0.0036 & 0.0036 & -0.4750 \\ 0.0715 & 0.0715 & 0.153 \\ 0 & 0 & 0 \\ 0 & 0 & 0 \end{bmatrix}.
$$

Figure 1-11. A and B state space numerical matrices [2].

1.9 Aircraft Stability Analysis

By calculating the eigenvalues of our linearized system's "**A**" matrix, the poles and zeros of the system can be determined in addition to its longitudinal and lateral properties being studied. In this

section we will review the open-loop stability characteristics of the linearized transport model. The poles and zeros will be plotted and explained in relation to a set of modes inherent to conventional aircraft. Following the pole zero analysis these modes are demonstrated via an open loop response to actuator impulses. These actuator impulses expose the marginally stable and unstable modes inherent to conventional aircraft. These results are shown in Figures 1-12, 1-13, and 1-14.

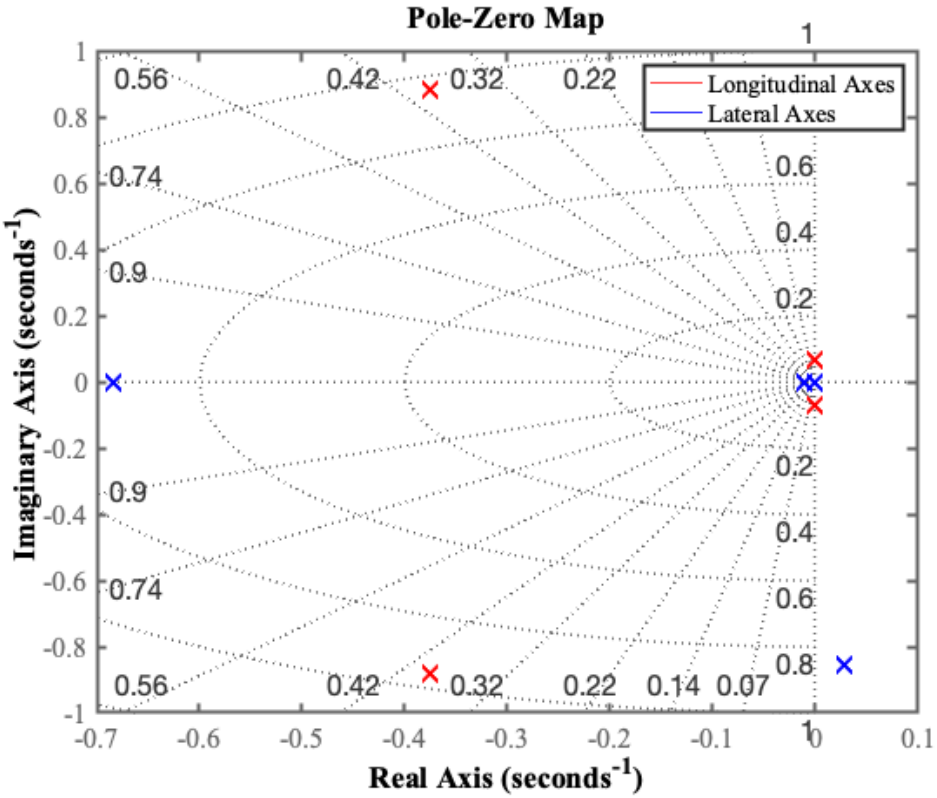

Figure 1-12. Pole-Zero Plot

Longitudinal Modes

The longitudinal poles are depicted by the red markers in Figure 1-12. This aircraft's longitudinal stability characteristic equation (eq 1.52) is 4th order. Its damping and natural frequency constants

denote both a Phugoid mode and Short-Period mode. Both of which, will need to be compensated for during nominal and adaptive controller design. [4], [5]

The phugoid mode appears as a long slow-moving oscillation with very little or no damping depending on aircraft characteristics. The Figure 1-13 demonstrates the phugoid mode after a 3-degree pulse of the elevator. The pitch of the aircraft begins a long period oscillation after the 20 second mark.

$$(\lambda^2 + 2\zeta_{ph}\omega_{ph}\lambda + \omega_{ph}^2)(\lambda^2 + 2\zeta_{sp}\omega_{sp}\lambda + \omega_{sp}^2) = 0 \tag{1.52}$$

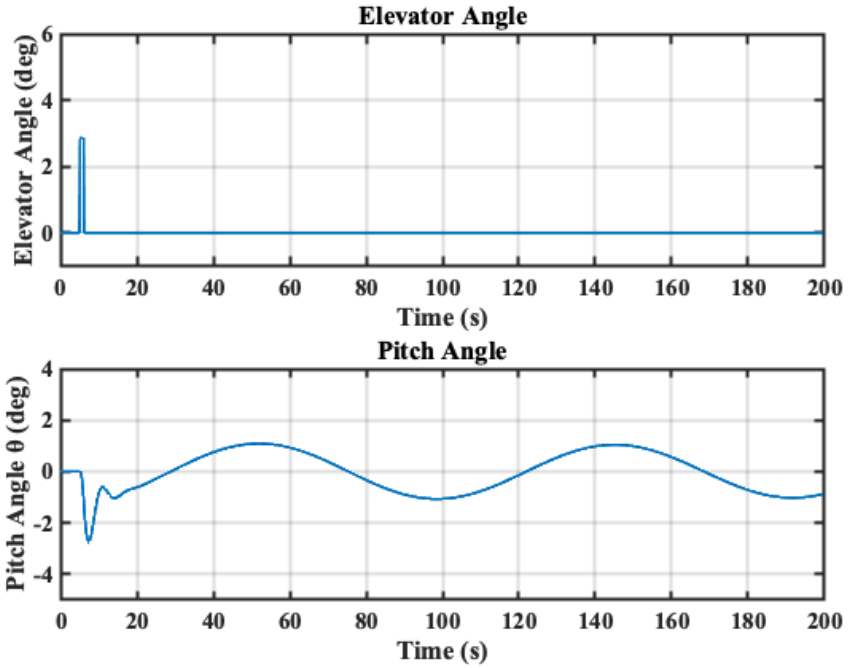

Figure 1-13. Open-loop pitch angle response to elevator pulse

The short period mode is a well damped oscillation that is seen just after the elevator pulse at the 5 second time mark. As shown in Figure 1-13 the short period mode is quickly damped while the phugoid mode becomes dominant in the open loop longitudinal dynamics.

Table 1-2. Longitudinal pole locations.

Pole	Damping	Frequency	Time Constant
		(rad/Time Unit)	(Time Unit)
-3.75e-01 + 8.82e-01i	*3.91e-01*	*9.58e-01*	*2.67e+00*
-3.75e-01 - 8.82e-01i	*3.91e-01*	*9.58e-01*	*2.67e+00*
-4.58e-04 + 6.74e-02i	*6.80e-03*	*6.74e-02*	*2.18e+03*
-4.58e-04 - 6.74e-02i	*6.80e-03*	*6.74e-02*	*2.18e+03*

In Table 1-2 the pole locations for the longitudinal axis are displayed. Here it is shown that the phugoid frequency is specified by the conjugate pairs closest to the imaginary axis. The phugoid mode parameters are ω_{ph}= 0.0674 rad/sec and ζ_{ph}= 0.00680. The short period mode, which is well damped is described by the remaining two poles. ω_{sp} = .958 rad/sec and ζ_{sp} = .391. [4], [5]

Lateral Modes

The lateral characteristic equation of this aircraft is 5th order (eq 1.53). One of the roots of this equation is a pure integrator and resides directly on the pole zero plot origin. The blue markers in Figure 1-12 denote the lateral system poles. The lateral modes in conventional aircraft display 3 unstable tendencies referred to as the spiral mode, subsidiary roll, and Dutch roll. In the figure below all three of these modes are displayed after a 3-degree pulse of the rudder at 5 seconds. This shows that the lateral axis open loop system is unstable without proper control. [4], [5]

$$\lambda(\lambda + e)(\lambda + f)(\lambda^2 + 2\zeta_D\omega_D\lambda + \omega_D^2) = 0 \quad (1.53)$$

Table 1-3. Lateral system pole locations.

Pole	Damping	Frequency	Time Constant
		(rad/Time Unit)	(Time Unit)
2.89e-02 + 8.54e-01i	*-3.38e-02*	*8.54e-01*	*-3.46e+01*
2.89e-02 - 8.54e-01i	*-3.38e-02*	*8.54e-01*	*-3.46e+01*
-6.84e-01	*1.00e+00*	*6.84e-01*	*1.46e+00*
-9.89e-03	*1.00e+00*	*9.89e-03*	*1.01e+02*

The lateral system pole locations shown in Table 1-3 display a conjugate pair related to the Dutch roll characteristics. The remaining two poles describe the spiral mode and subsidiary mode that give the lateral system its unstable open loop characteristics.

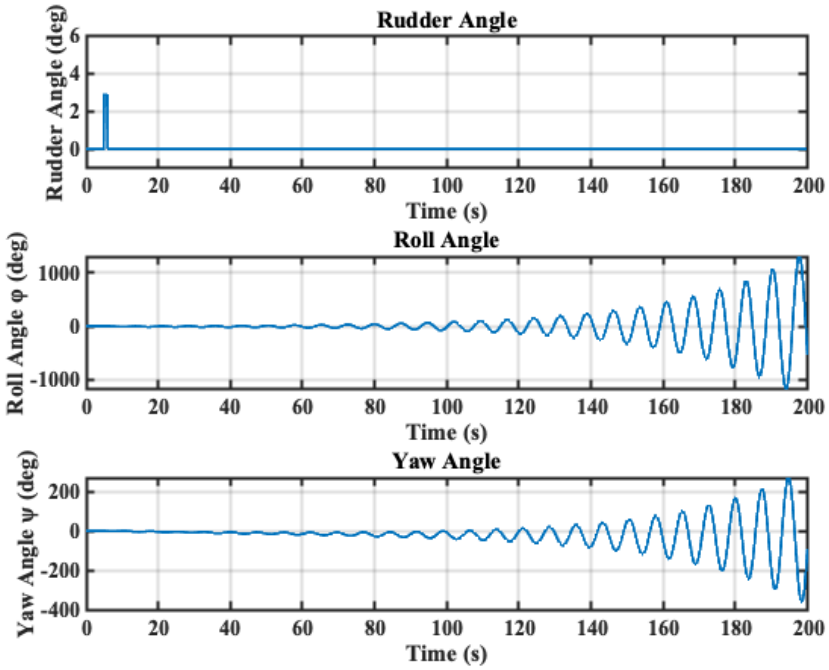

Figure 1-14. Open-loop lateral response to rudder pulse

Chapter 2

Nominal Controller Design

This section will review the nominal controller design. This controller will dictate the transient and steady state dynamics of the model reference in addition to being used as a baseline in the adaptive controlled plant. First, an LQR controller is integrated as a feedback loop in the 9th order aircraft system. The cost function is then modified to maximize inherent system properties and minimize the excitation of modes described in section 1.9.

2.1 Linear Quadratic Regulator

An LQR controller is advantageous to a pole placement or PID controller for a range of reasons. At first look, a pole placement loop will yield faster rise times and shorter time to system stability. However, when examined closer and integrated with control surface saturation and rate saturation blocks, control surfaces become quicky saturated and lead to system instability or even system damage. This is the root of the use case for an optimum control scheme.

In this case the dynamic process to be controlled is the 9th order differential thrust transport aircraft model. The process is modeled with the following state space equation.

$$\dot{x} = Ax + Bu \tag{2.1}$$

Where, x is the state vector, u is the control input, and A and B are as defined in chapter 1. The goal is to seek an optimal control law u_c defined here.

$$u_c = Kx \tag{2.2}$$

Where $K \in R^{6x9}$ is a feedback gain matrix which minimizes the quadratic performance index described by J. [2]

$$J = \int_0^\infty (x^T Q x + u^T R u)\, dt \tag{2.3}$$

And Q and R are symmetric matrices.

These matrices are usually called the "state weighting matrix" and the "control weighting matrix," respectively. Formulating the control problem in terms of a quadratic cost function allows the controller to minimize control effort and maximized desirable response characteristics. In the cost function described above, the two terms ($x^T Q x$ and $u^T R u$) form what is called the "integrated cost of control." The next section will describe how the cost of control is shaped in respect to the system of interest [6].

2.2 Cost Function Tuning

In the assessment of the cost function the term $x^T Q x$ represents a penalty on the deviation of the state from the trimmed condition while $u^T R u$ represents the "cost of control." In accordance with how we have defined the steady state condition, the desired state of the system is the origin (zero state vector) [6].

The relationship between the weighting matrices and the dynamics of the closed loop system are complex. It is not an effective practice to draw conclusions for the performance of the closed loop system solely based on the weighting matrices. Therefore, the tuning of the LQR controller, was

accomplished via trial and error in addition to considering inherent aircraft and actuator dynamics. The approach used solves for the gain matrix K resulting from a set of Q and R iterations. The corresponding closed loop responses to the gain matrices are simulated in MATLAB and the weighting matrices corresponding to the most desired effects are selected.

This controller is designed for an infinite control interval. A control gain matrix K must be found to minimize the performance integral defined in equation 2.3.

If the performance is integrated backwards in time, it will either converge to a constant matrix P or grow unbounded. If the integral converges to a limit its derivative will be zero. Therefore

$$J_\infty = x'Px \tag{2.4}$$

Where P satisfied the algebraic Riccati equation (ARE)

$$A^TP + PA - PBR^{-1}B^TP + Q = 0 \tag{2.5}$$

And the optimum steady state gain is given by

$$K = -R^{-1}B^TP \tag{2.6}$$

Given these formulations a few conditions need to be met. For the ARE to have a unique positive definite solution P which minimized J, the following criteria must be met.

1) The system must be asymptotically stable or [6],
2) The system must be controllable and observable [6].

Figures 2-1, 2-2, 2-3, and 2-4 outline a state and control output comparison. The plots compare using an Identity matrix of appropriate dimensions for Q and R with a system specific weighting of Q and R matrices.

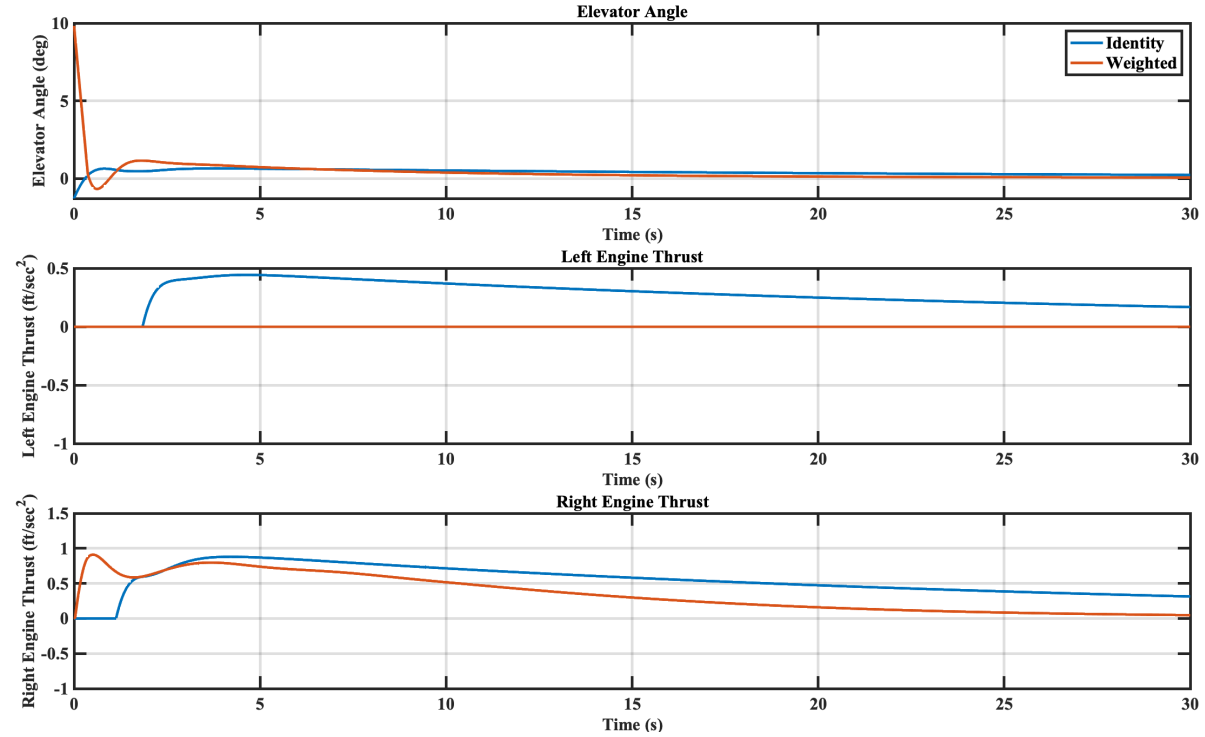

Figure 2-1. System inputs (top to bottom) $u_1 = \delta_e$, $u_2 = \delta_{t_l}$, $u_3 = \delta_{t_r}$.

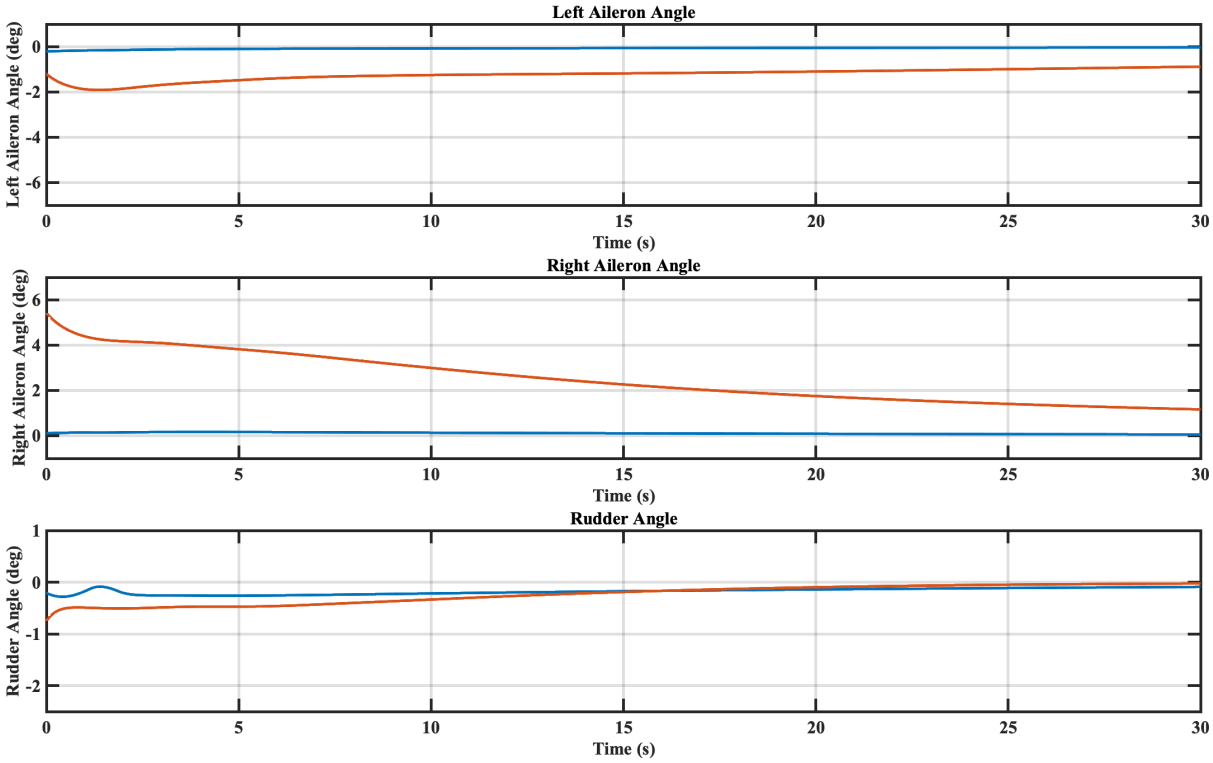

Figure 2-2. System inputs (top to bottom) $u_4 = \delta_{a_l}$, $u_5 = \delta_{a_r}$, $u_6 = \delta_r$.

For the Q matrix weighting, large conventional aircraft dynamics were considered. The most heavily penalized state error is x_5 which describes the aircrafts lateral velocity. As demonstrated in Chapter 1 the lateral axis is inherently unstable. By penalizing state variables that are most likely to excite the Dutch roll and spiral modes, the controller will be able to execute improved performance over a broader range of flight conditions.

$$V = [1 \quad 1 \quad 0 \quad 30 \quad 1 \quad 0 \quad 0 \quad 30 \quad 30] \tag{2.7}$$

$$Q = diag\{V\} \tag{2.8}$$

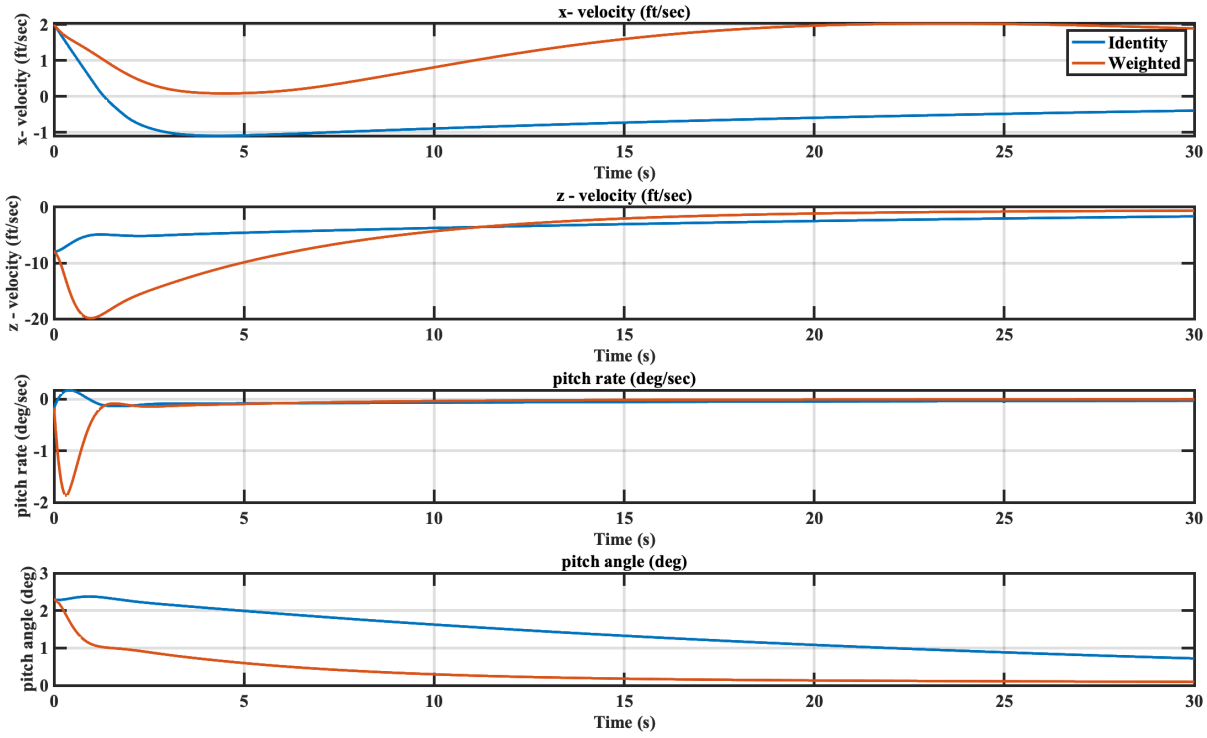

Figure 2-3. System states (top to bottom) $x_1 = u$, $x_2 = w$, $x_3 = q$, $x_4 = \theta$

When tuning the R matrix (eq 2.11 & 2.10), real world actuator dynamics and aircraft characteristics are considered. An aircraft pilot's first choice of flight controls will always be

ailerons to control lateral movement and elevator to control vertical movement. This is reflected in the weighting of the R matrix along the main diagonal.

$$M = [1 \quad 10 \quad 10 \quad 1 \quad 1 \quad 10] \tag{2.11}$$

$$R = diag\{M\} \tag{2.10}$$

Considering the longitudinal and lateral coupled model, the rudder and engine thrusts induce movements in multiple axis which complicates the control solution. These control surfaces will become an important part of the adaptive controller however, in the nominal design, penalizing their use provides for improved performance.

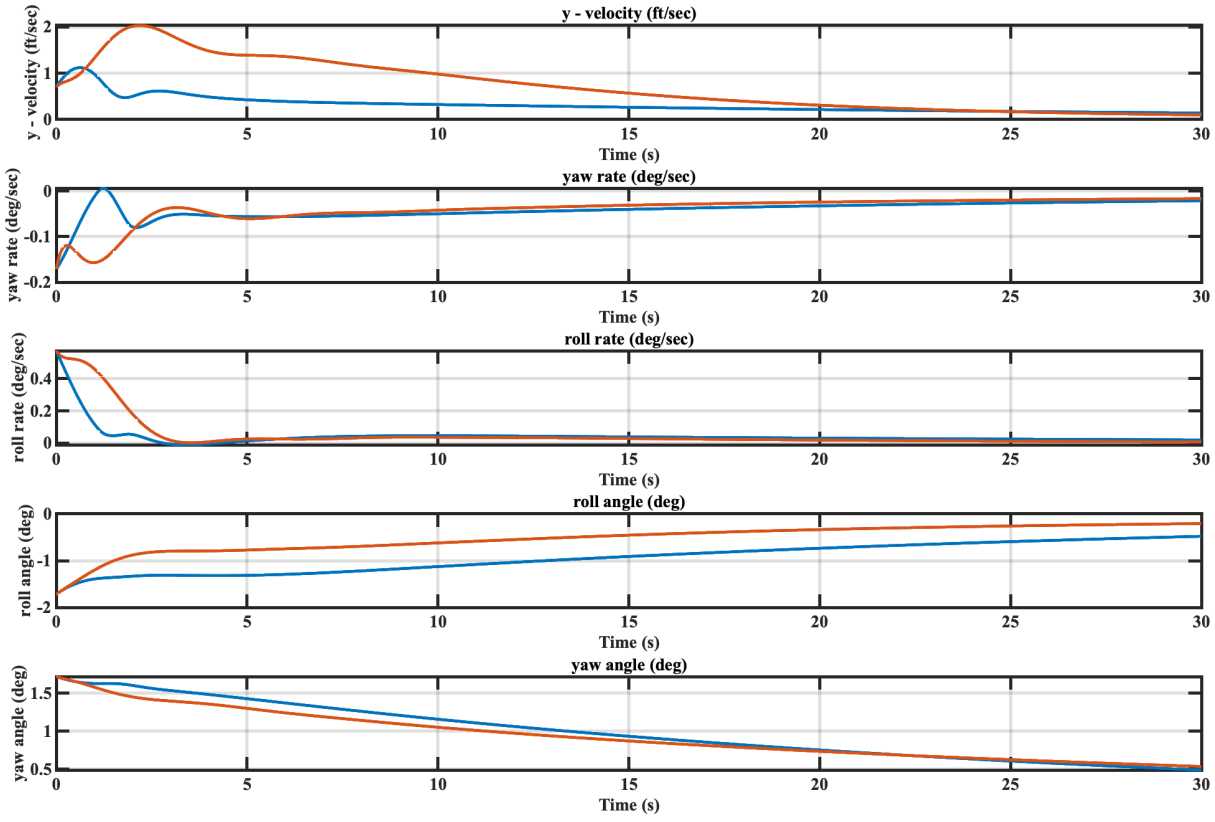

Figure 2-4. System states (top to bottom) $x_5 = v$, $x_6 = r$, $x_7 = p$, $x_8 = \phi$, $x_9 = \psi$

2.3 Controller Performance and Stability

After using the weighting methodology for the LQR controller matrices outlined in the previous section, a nominal simulation was run with a fully functioning aircraft model. Figures 2-1 through 2-4 compare an LQR controller with equal weighting to another controller with the weighted Q and R matrices outlined in section 2.2.

Chapter 3

Adaptive Controller

Adaptive control research started in the early 1950's specifically, for the design of autopilots in high performance aircraft. Its application was created to compensate for wide ranges in speeds, altitudes, and gravity force loading ("G-loading"). The core idea in adaptive control is to estimate certain "on-line" system parameters based on output feedback or some other system measurement. The main difference in an adaptive controller is that its parameters are variable in conjunction with the system behavior and desired state. In this section the classical method known as the "MIT rule" will be implemented into the 9^{th} order state space model to overcome different sets of aircraft actuator failures. [7]

The full adaptive scheme will consist of a plant, reference model, controller, and adaptation mechanism. These elements work in conjunction to ensure system boundedness and stability.
In an MRAC controller the reference model is used to dictate the ideal response of the adaptive system. The plant augmented in this paper is a steady state trimmed aircraft model with a perturbed flight condition as its initial state. Therefore, the reference model will dictate the ideal reaction to this perturbed flight condition as the reference model corrects back to level unaccelerated slight. It is important for the reference model to display the desired parameters of the overall adaptive system, this includes actuator employment, rise time, setting time, and overshoot. Chapter 2 outlined the design of the reference model and its controller. Here the paper will outline the design of the controller and adaptation mechanism. [7]

The adaptive controller consists of a state feedback loop with a set of adjustable parameters. The goal for this controller is to have the ability to perfectly track the reference model allowing the tracking error to converge to zero. When the actuator failures are implemented, the adaptive controller will adjust its parameters to achieve perfect tracking asymptotically. Given that the nominal controller is an LQR design, stability and tracking convergence are guaranteed. This is further demonstrated in section 3.3. [7]

3.1 Actuator Failures

To test the adaptive element of the controller, the ability to fail control surfaces needs to me implemented into the state space and Simulink models. The mathematical integration also plays an important role in proving system boundedness and convergence. The state space model begins as in Chapter 1.

$$\dot{x} = Ax + Bu, \quad x \in R^n, u \in R^m, \tag{3.1}$$

Actuators $u = [u_1 \quad u_2 \ldots u_m]^T$ may fail to zero or an unknown constant during operation. In the event of actuator failure at a fixed position, the failed actuator constant is represented by the following control matrix. Therefore

$$u_i(t) = \bar{u}_i, t \geq t_i, i \in \{1,2, \ldots m\}, \tag{3.2}$$

Where t_i is the time at which the failure occurs and u_i is the unknown control surface position. This would be the case when an aircraft control surface becomes stuck in a fixed position. This is also known as control binding and, it become applicable in runaway trim scenarios.

In the presence of control surface failures, the input vector and the overall system are represented by the following state space equations. [2]

$$u(t) = v(t) + \sigma(\bar{u} - v(t)), \tag{3.3}$$

$$\sigma_i = \begin{cases} 1 \; if \; the \; i^{th} \; actuator \; has \; failed \\ 0 \; otherwise. \end{cases} \tag{3.4}$$

$$\dot{x}(t) = Ax(t) + B(I - \sigma)v(t) + \sigma B\bar{u}. \tag{3.5}$$

3.2 Adaptation Laws

The adaptive controller will vary its parameters to achieve perfect tracking asymptotically via its adaptation mechanism or adaptation law. This law searches for parameters so the response of the 9th order aircraft system tracks to the response of the reference model. This is the main differentiator from conventional control. In this paper Lyapunov theory will be the formalism of choice to prove stability. Mathematically proven stability has shown to be the most trusted way to prove safety in the aerospace industry. [7]

Assumption 3.1 (A, B) is stabilizable, and rank [$B(I - \sigma)$] = rank [B], for all $\sigma \in \Sigma$, where $\Sigma \subset \bar{\Sigma}$ is the set of actuator failure patterns deemed recoverable [2].

The following control law is chosen to achieve asymptotic tracking of the nominal controller,

$$v_d(t) = \hat{K}x(t) + \hat{\theta}, \tag{3.6.1}$$

where,

$$\hat{K} = [\hat{K}_1, \hat{K}_2, \ldots, \hat{K}_m]^T \in R^{m \times n}, \tag{3.6.2}$$

and,

$$\hat{\theta} = [\hat{\theta}_1, \hat{\theta}_2, \ldots, \hat{\theta}_m]^T \in R^{m\times 1}. \tag{3.7}$$

In addition, the adaptive laws are chosen as follows.

$$\dot{\hat{K}}_i = -\Gamma_i\, x\, e^T \boldsymbol{P}\, b_i,\ i = 1,2,\ldots m \tag{3.8}$$

$$\dot{\hat{\theta}}_i = -\lambda_i\ e^T \boldsymbol{P}\, b_i,\ i = 1,2,\ldots m \tag{3.9}$$

where $\Gamma_i = \Gamma_i^T > 0, \lambda_i > 0, b_i\ is\ the\ ith\ column\ of\ B, i = 1,2,\ldots,6, and\ P = P^T > 0$ such that

$$A^T\boldsymbol{P} + \boldsymbol{P}A - \boldsymbol{P}BR^{-1}B^T\boldsymbol{P} + Q = 0. \tag{3.10}$$

When referencing the 9th order aircraft model m = 6 representing the 6 control inputs while n = 9 representing the 9 states describing the system [2].

Γ_i, and λ_i are positive definite and denote the design parameters for the adaptive laws. $\hat{K}$ uses the Γ_i to attempt to match the gain K calculated in Chapter 2. In this case Γ_i is a 9x9 square matrix whose diagonal contains the traditional adaptive gain for its respective state. In the results section it is shown how the values of $\hat{K}$ will attempt to match the gains of the ideal calculated LQR gain matrix. $\hat{K}$ by itself will not compensate for an actuator failure as it still programs control usage of the failed actuators.

$\hat{\theta}$ is core to the adaptive mechanism. It will use the error between the reference model and the plant in conjunction with the λ_i learning rates to drive the plant back to steady state. $\hat{\theta}$ is the adaptive mechanism that causes convergence in the face of actuators using the remaining control services. Using the error variable, it adaptively increases the gains of working control actuators. This enables system stability and convergence to steady state as outlined in section 3.3.

3.3 Lyapunov Stability Analysis

As mentioned earlier in the paper the 9th order system has been linearized using small perturbation theory. However, the addition of the adaptive controller makes the system error dynamics inherently nonlinear. Proving system stability is imperative for real world use. An unstable or unbounded control system can yield dangerous outcomes. Therefore, to prove output boundedness, Lyapunov theory is used.

The aircraft system is trimmed at the start of the simulation at an equilibrium point described in Chapter 1. The aim of this section is to prove stability and boundedness around that equilibrium point.

Here uniform continuity is examined by determining where a differentiable function has a bounded derivative.

As in [2] a Lyapunov function candidate is selected.

$$V = e^T \boldsymbol{P} e + \sum_{i \neq i_1,\ldots,i_p} (\widehat{K}_i - K_i)^T \Gamma_i^{-1} (\widehat{K}_i - K_i) + \sum_{i \neq i_1,\ldots,i_p} \lambda_i^{-1} (\hat{\theta}_i - \theta_i)^2 \qquad (3.11)$$

Where $p<m$ denotes the number of actuator failures and Γ and $\boldsymbol{P}$ are positive definite constant matrices. P satisfies

$$A^T \boldsymbol{P} + \boldsymbol{P} A = -Q \quad Q = Q^T > 0. \qquad (3.12)$$

for a chosen Q. The derivative $\dot{V}$ is then calculated as in [2]. Therefore, the time derivative for the time interval used for simulation is

$$\dot{V} = -\boldsymbol{e^T Q e} \leq 0. \tag{3.13}$$

Lemma 3.1(Barbalat's Lemma) If the differentiable function f(t) has a finite limit as t $t \rightarrow \infty$ *, and if* $\dot{f}$ *is uniformly continuous, then* $\dot{f}(t) \rightarrow 0 \; as \; t \rightarrow \infty$ [2].

Using this lemma convergence is shown. With the control law and adaptive law defined above the error and its (n-1) derivatives converge to zero therefore proving boundedness. The proof for this claim is found in [2][8].

Chapter 4

Simulation

This Chapter will review the implementation of the aircraft model, nominal controller, and adaptive controller in MATLAB and Simulink.

4.1 Model Overview

The aircraft model in chapter 1, nominal controller in chapter 2, and adaptive controller described in chapter 3 are all implemented for simulation with MATLAB and Simulink. This section will describe how each model element was integrated into the simulation and how the simulation results mirror some real-world aspects of an adaptive controller.

The system overview contains three main design blocks in addition to an error summation and output sinks. The system is broken into the reference model (shown in blue), the plant (green), and the adaptive controller. The reference system will contain the nominal aircraft model developed in chapter 1 and the nominal controller developed in chapter 2. The purpose of the reference system is to provide an output of a fully functioning 9^{th} order model with no actuator failures.

The plant contains the aircraft model and nominal controller but, it will take inputs from the adaptive element. The plant design block will also have an actuator saturation and failure block to simulate actuator failures unknowingly to the adaptive controller.

Lastly, the adaptive controller contains the implementation of the two adaptive laws and control law outlined in chapter 3. This block is the focal point for this paper as it is responsible for compensating for the simulated actuator failures.

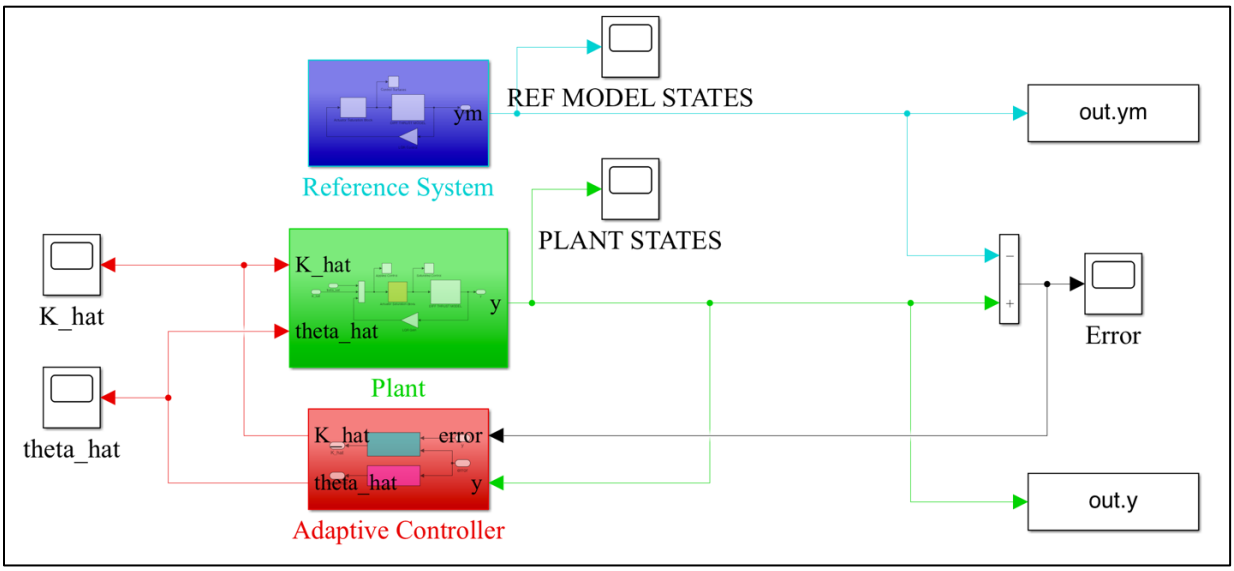

Figure 4-1. Model overview

4.2 Initial Conditions

The control objective of this simulation is to return the system back to its steady state at the origin of the state vector. *i.e.,* $x = [0 \quad 0 \quad 0 \quad 0 \quad 0 \quad 0 \quad 0 \quad 0 \quad 0]^T$. Therefore, the simulation's initial condition is a perturbed state vector. In the results section we will use the following initial condition. [2]

$$x_0 = [2 \quad -8 \quad 0.3 \quad 4 \quad 0.7 \quad -0.3 \quad 1 \quad -3 \quad 3]^T \tag{4.1}$$

The physical meaning of the initial condition is the aircraft in a 2 ft/sec velocity perturbation on the x-axis, at 8 ft/sec velocity perturbation on the z- axis, and a 0.7 ft/sec velocity perturbation on the y-axis. Both the yaw and pitch rates are -0.3 crad/sec corresponding to a slight descending left tendency for the aircraft. Finally, the roll rate is 1 crad/sec with a yaw angle of 3 crads (1.72 eg) [2].

$$x_d = [4 \quad -1.06 \quad 0 \quad 1 \quad 0 \quad 0 \quad 0 \quad 0 \quad -1.8]^T \tag{4.1.1}$$

In some of the simulations an alternate steady state condition will be defined through a desired state vector. This trajectory represents a flight condition in which the aircraft is climbing at 4 ft/sec velocity perturbation along the x-axis, a -1.06 ft/sec velocity perturbation along the z-axis, a pitch angle of 1 crad and a yaw angle of 1.8 crad. The initial conditions vectors for these simulations will be zero. i.e., a steady state wings level flight condition [3].

4.3 Actuator Model

When modeling real world characteristics of an aircraft the maximum control surface deflections and maximum rates at which the surfaces deflect is critical in controller development. When aircraft pilots manually control aircraft, they face the same challenge. At slower airspeeds and higher altitudes control surface effectiveness and the rate at which they deflect can be a limiting factor when maneuvering the aircraft.

These aspects are integrated into the reference model and the plant with the actuator block depicted below.

Each of the six control inputs have a deflection limit block and rate limit block. These limits will be specified in the results section and will differ based on the design case at hand. The actuator block is also used to implement the control surface failures. Since they are modeled with a zeroizing step function, the surface failure is unknown to the controller. The step blocks are programmed to multiply the scheduled control input by 0 at the specified failure time (t_f). This thereby removes any effect that control surface had on the system after t_f.

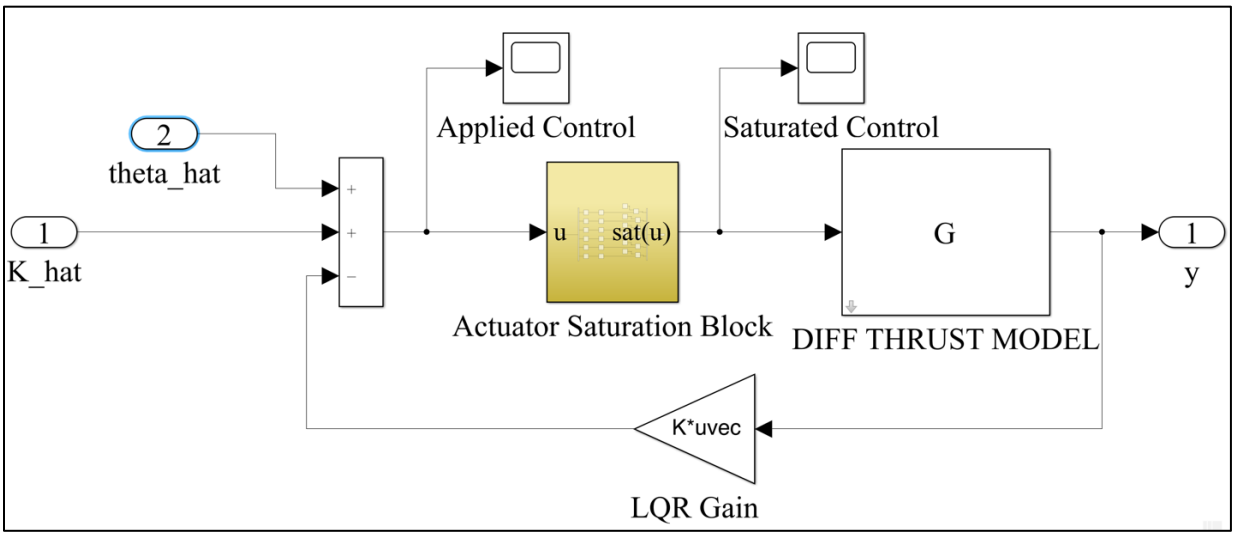

Figure 4-2. Plant block overview

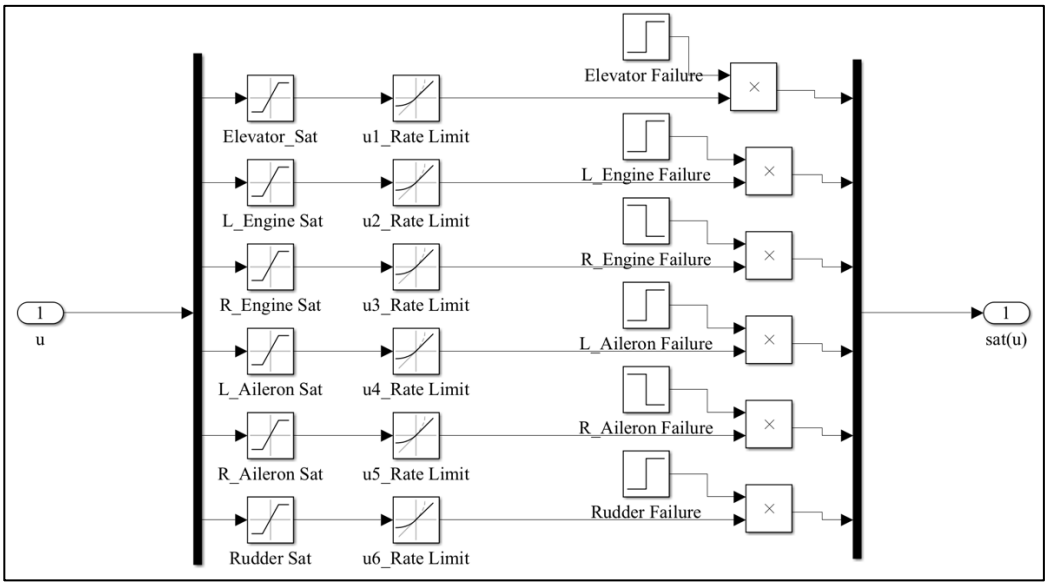

Figure 4-3. Control saturation block

4.4 Model Reference

The reference model is used as a comparison to the plant output. The error between these two blocks is then routed as an input to the adaptive element of the adaptive controller. The reference model consists of the aircraft model developed in Chapter 1, the LQR controller designed in

Chapter 2, and the actuator saturation block outlined in the previous section. The goal is to have the adaptive controller asymptotically approach the output of the reference model shown in Figure 4-4.

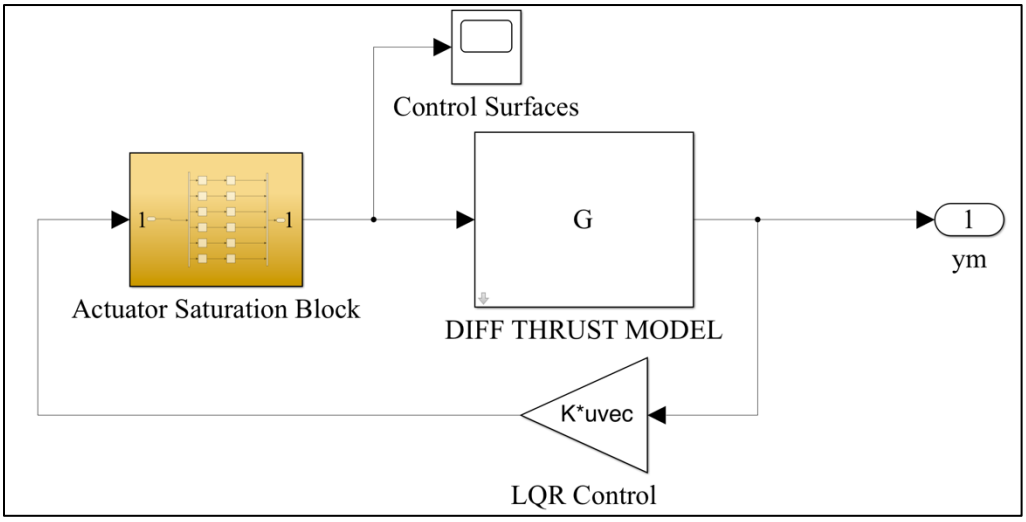

Figure 4-4. Reference model block

4.5 Adaptive Controller Implementation

The adaptive controller is composed of two elements as shown in Figure 4-5. These elements are the implementations of the adaptive laws outlined in Chapter 3. The outputs of these blocks are routed as inputs to the plant allowing it to adaptively compensate for actuator failures. Figures 4-6 and 4-7 show how the adaptive laws form Chapter 3 were implemented.

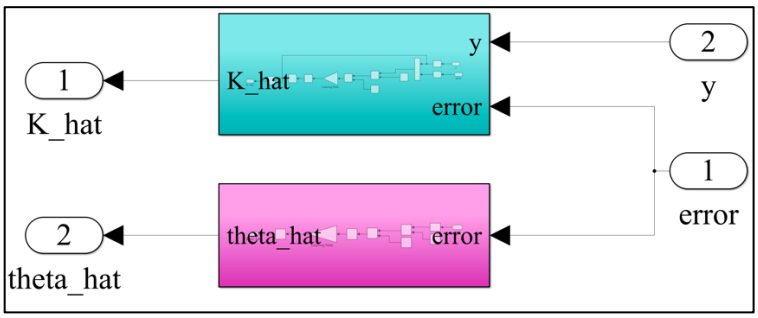

Figure 4-5. Adaptive controller block

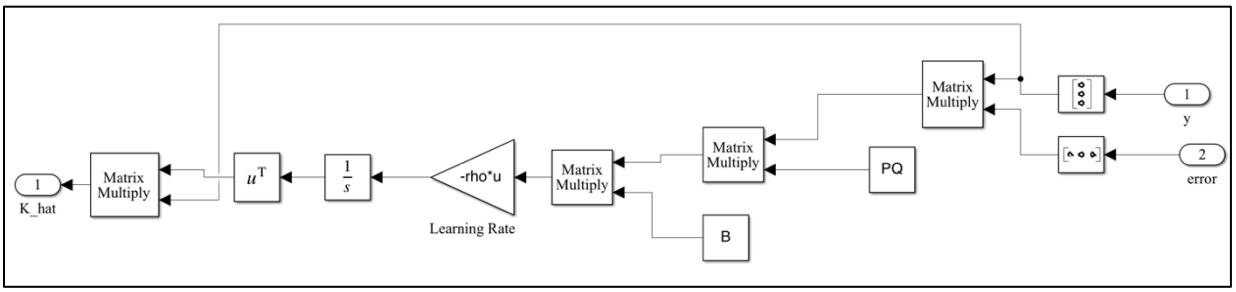

Figure 4-6. $\dot{\hat{K}}_i$ Adaptive law implementation

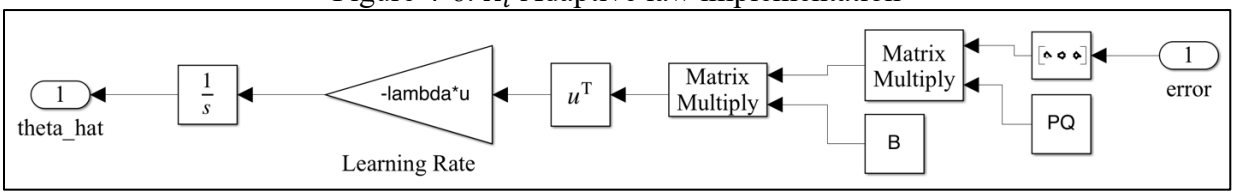

Figure 4-7. $\dot{\hat{\theta}}_i$ Adaptive law implementation

Chapter 5

Results

The results will display the state output of the 9th order aircraft plant in relation to the 9th order reference model. All plots in this section have a failure time of 0 seconds. In other words, the failures occur instantaneously and renders the control surface to a zero-deflection angle. Each plot will display two lines. The blue line ("xm" followed by the state number) represents the desired response outlined by the reference model output. The orange line ("x" followed by the state number) will represent the output of the plant under the constraints of the specific case.

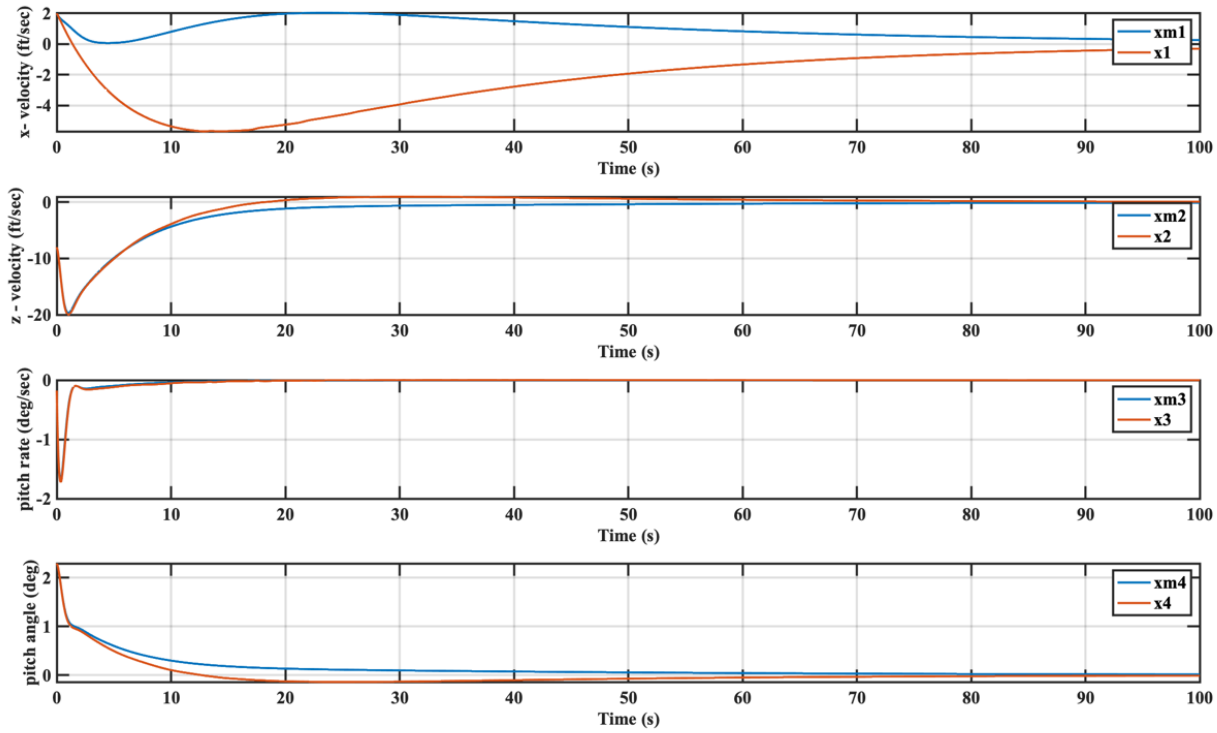

Figure 5-1. System states (top to bottom) $x_1 = u$, $x_2 = w$, $x_3 = q$, $x_4 = \theta$ (Case I)

5.1 Case I

Case I will show the performance of only the nominal controller during a right thrust and right aileron failure. As previously mentioned, the LQR based nominal controller does not deal with actuator failures acceptably. The state outputs for Case I are shown in figures 5-1 and 5-2.

The failure pattern presented to the nominal controller is recoverable. The failure of a right engine thrust, and a right aileron will yield a mostly lateral control problem. For states 1-4 in Figure 5-1 the z-velocity, pitch rate, and pitch angle all track relatively well to the reference model despite the failures. This is due to the longitudinal system largely being unaffected apart from the deviation in x-velocity (forward velocity). This is clearly due to the thrust suddenly being cut in half due to the right engine failure.

Figure 5-2 shows the failure pattern's effects on the longitudinal portion of the system. The nominal controller's performance with actuator failures does converge but yields undesirable system effects. The roll rate and yaw rate oscillate significantly while the roll angle and yaw angle also oscillate. This sort of excitation after an actuator failure yields a semi-unstable system and can excite unmodeled dynamics.

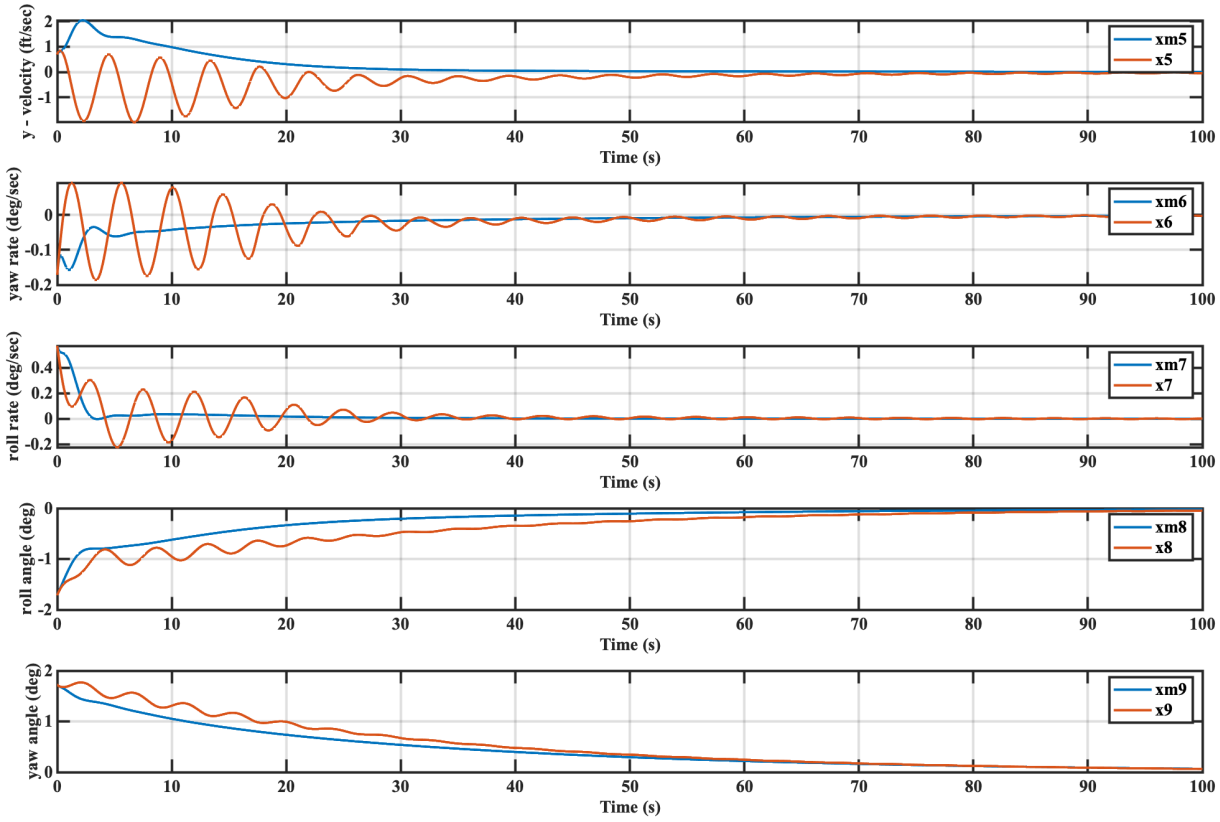

Figure 5-2. System states (top to bottom) $x_5 = v$, $x_6 = r$, $x_7 = p$, $x_8 = \phi$, $x_9 = \psi$ (Case I)

5.2 Case II

This case will display the advantages of using an adaptive controller. The system experiences an instantaneous rudder failure and right aileron failure. For this simulation $\Gamma = .001 \times I_{9x9}$ and $\lambda = [.001\ .005\ .005\ .002\ .002\ .002]$ as in [2]. These will be the baseline learning rates to which other cases are compared. The results are displayed in Figures 5-3 and 5-4.

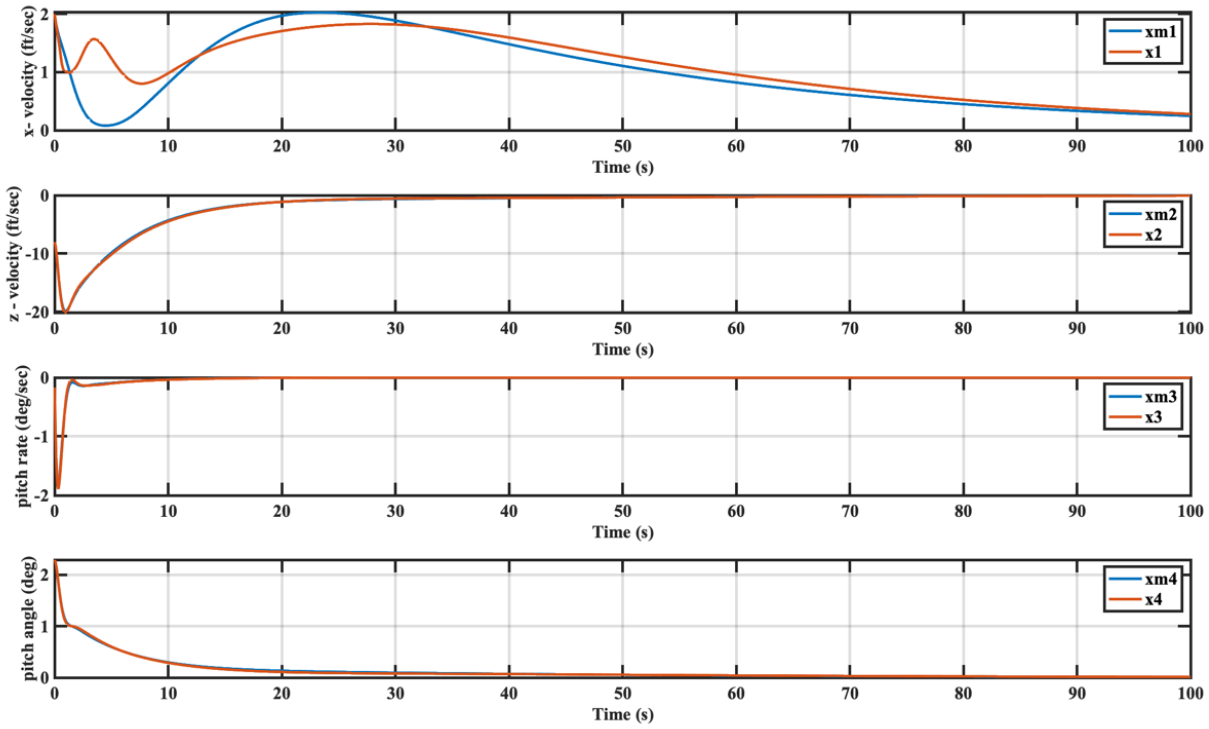

Figure 5-3. System states (top to bottom) $x_1 = u$, $x_2 = w$, $x_3 = q$, $x_4 = \theta$ (Case II)

Again, the failure pattern is largely a lateral control issue. With the failure of the rudder and right aileron asymmetric thrust will largely compensate for the loss of lateral control surfaces. The use of engine thrust variations to aid aircraft control is one of the strongest use cases for adaptive control [9]. As seen in Case I states 2-4 track very well. The longitudinal velocity fluctuates due to the use of engine thrust to compensate for reduced lateral control. Figure 5-4 shows how roll angle lags after the failure but adaptively converges along with the yaw angle. In this case all oscillatory behavior is terminated well before the 10 second mark. Speculatively this performance would outperform some pilots in the same failure scenario.

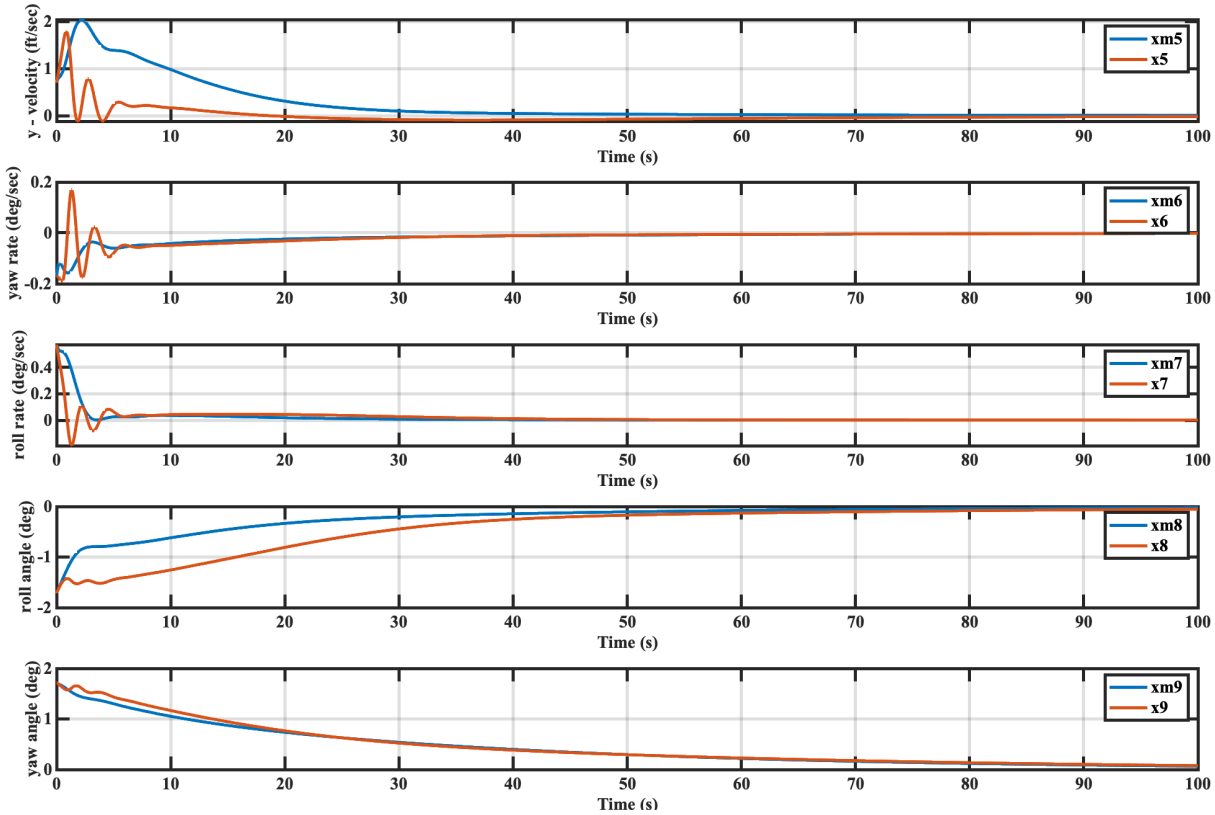

Figure 5-4. System states (top to bottom) $x_5 = v$, $x_6 = r$, $x_7 = p$, $x_8 = \phi$, $x_9 = \psi$ (Case II)

5.3 Case III

Case III will test the same adaptive controller from Case II with the same failure pattern from Case I. The system experiences an instantaneous right thrust and right aileron failure. In this case $\Gamma = .001 \times I_{9x9}$ and $\lambda = [.001\ .005\ .005\ .002\ .002\ .002]$ as in [2]. This Case directly shows the benefits of an adaptive controller in contrast to the nominal controller performance in Case I. The states shown in Figure 5-5 mostly match the performance of the nominal controller in Case I. Again, this is due to the failure scheme being a lateral control problem. As opposed to the nominal controller performance the adaptive controller achieves zero steady state error and convergence to the reference model about 25 percent faster. The most desirable trait is that the oscillatory motion

of the aircraft is stopped prior to 10 seconds after the actuator failures. We also see this demonstrated in Figure 5-6 although, the steady state error is not corrected as quickly.

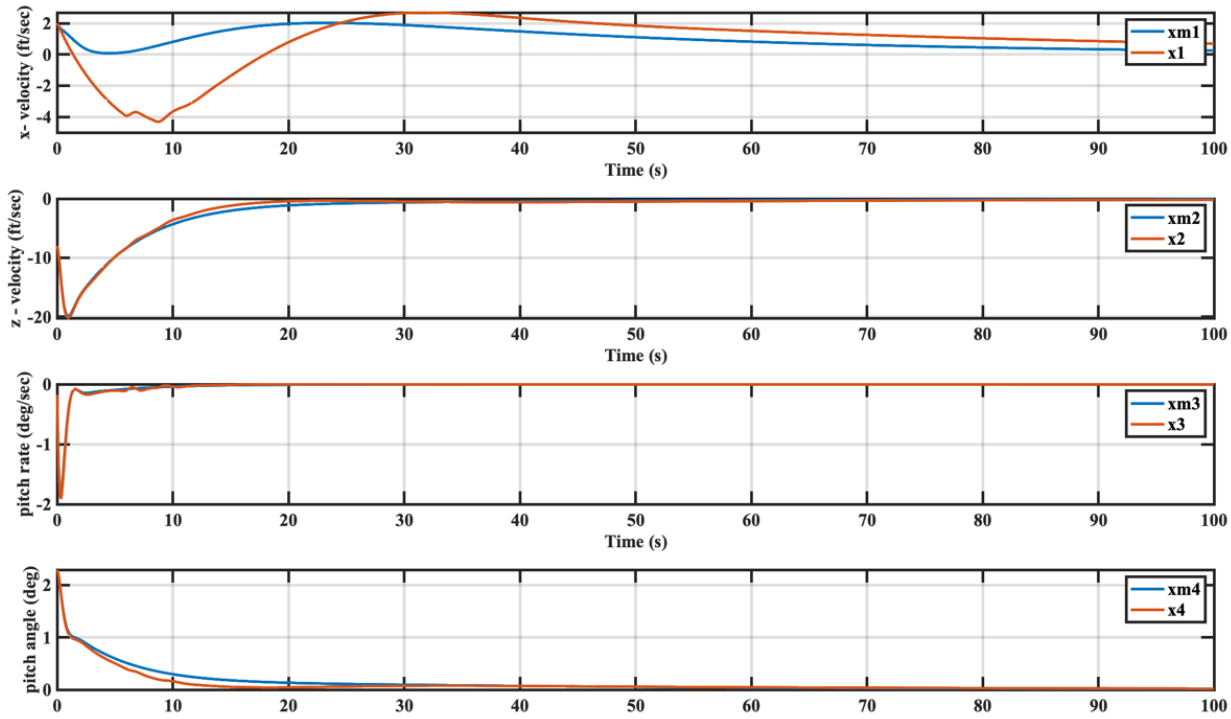

Figure 5-5. System states (top to bottom) $x_1 = u$, $x_2 = w$, $x_3 = q$, $x_4 = \theta$ (Case III)

5.4 Case IV

Case IV will test the adaptive controller with an increased learning rate. The system experiences an instantaneous rudder failure and right aileron failure. In this case $\Gamma = .003 \times I_{9x9}$ and $\lambda = [.01\ .05\ .05\ .02\ .02\ .02]$. Γ is three times as large as previous cases while λ is increased by a factor of ten. As shown in Figure 5-7, this is the first case to show improved tracking of the x-velocity state (x_1). This combination of learning rates was found during trial and error to maximize reference model state tracking while reducing control saturation. As is shown in Case VI increased learning rates can drive instability due to rate and deflection saturation of the control surfaces.

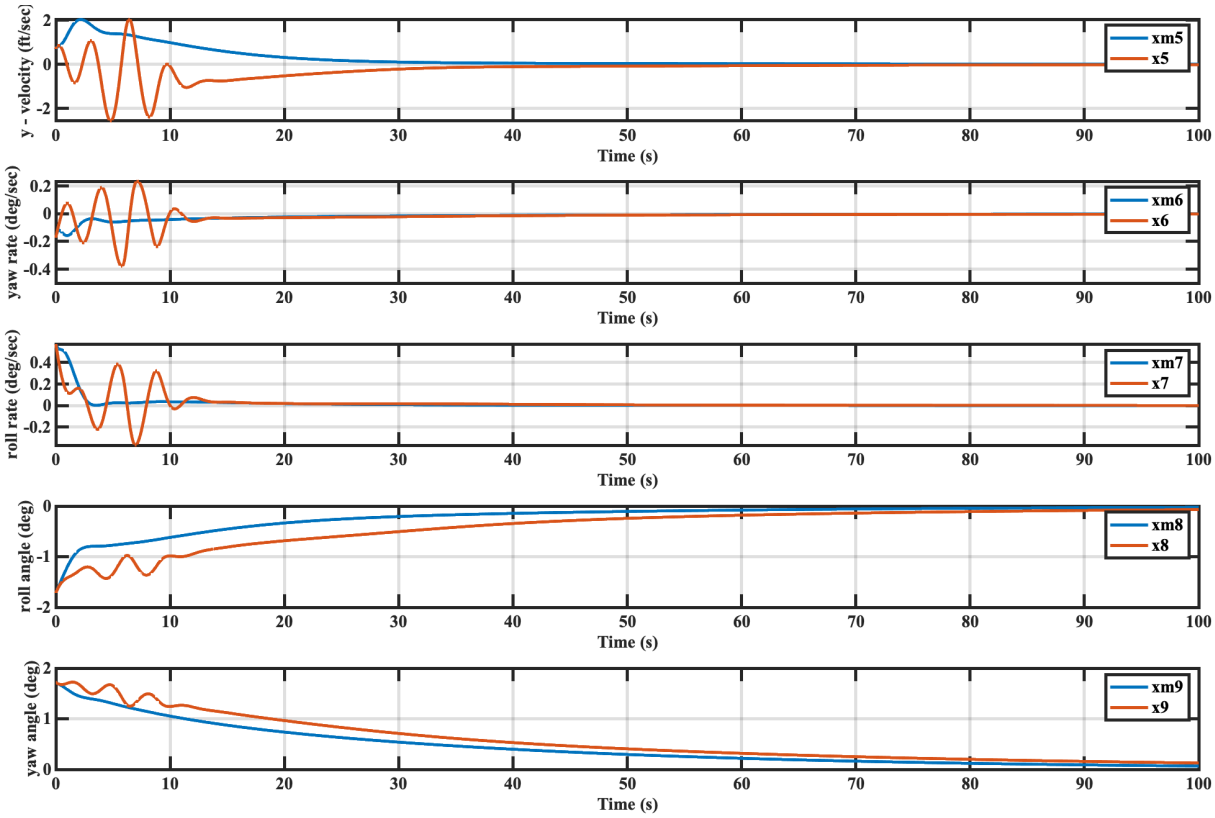

Figure 5-6. System states (top to bottom) $x_5 = v$, $x_6 = r$, $x_7 = p$, $x_8 = \phi$, $x_9 = \psi$ (Case III)

Figure 5-8 shows the response of the lateral aircraft system. The difference seen in this case is the behavior of the lateral velocities and angle rates. It is shown that the system more rapidly changes velocities to aid in attitude state tracking. This aligns with the design of our nominal and adaptive controller. In those sections the "penalty" for poor attitude tracking was weighed much higher than velocity tracking. This is a real-world practicality. It is clearly shown in Figure 5-8.

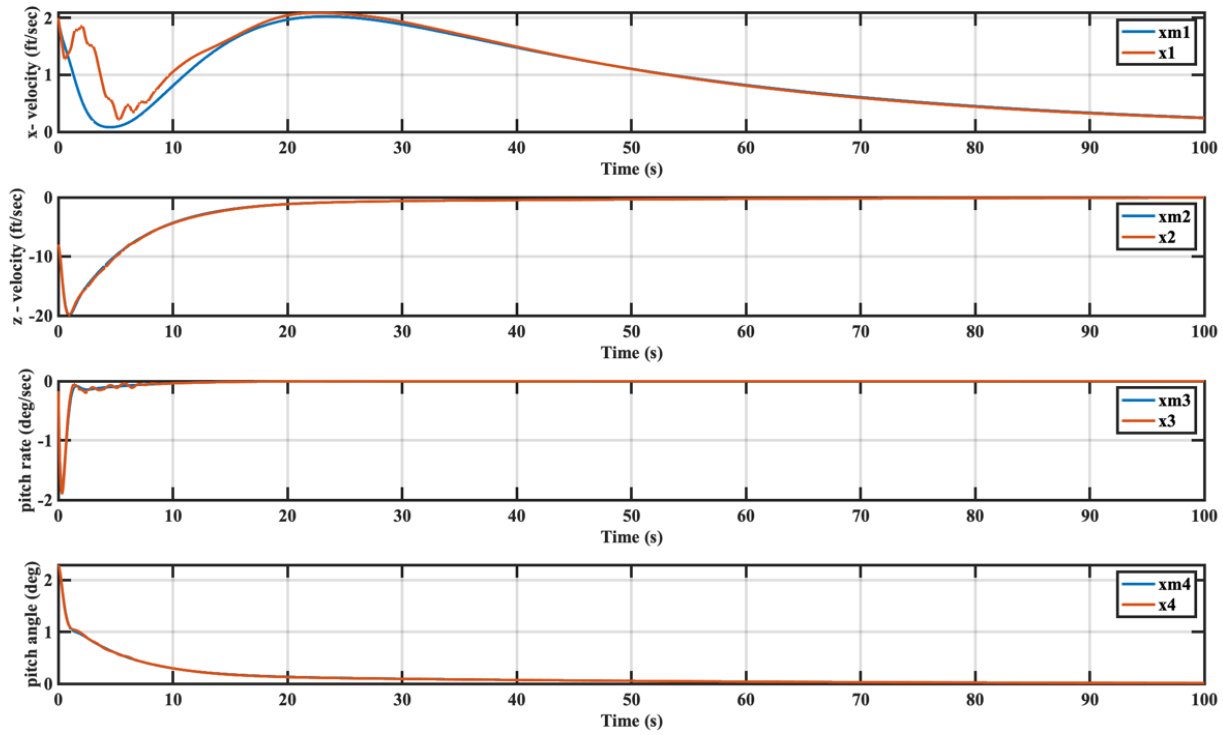

Figure 5-7. System states (top to bottom) $x_1 = u$, $x_2 = w$, $x_3 = q$, $x_4 = \theta$ (Case IV)

5.5 Case V

Case V will test the adaptive controller with an increased learning rate. The system experiences an instantaneous right thrust and right aileron failure. In this case $\Gamma = .003 \times I_{9x9}$ and $\lambda = [.01\ .05\ .05\ .02\ .02\ .02]$ as in [2]. Here it is shown the effect of an increased learning rate on the same conditions presented in Case III. The results are shown in Figures 5-9 and 5-10. Both figures show similar results to Case II with the additional "chattering" shown in the attitude state outputs. This is expected when increasing the adaptive gains.

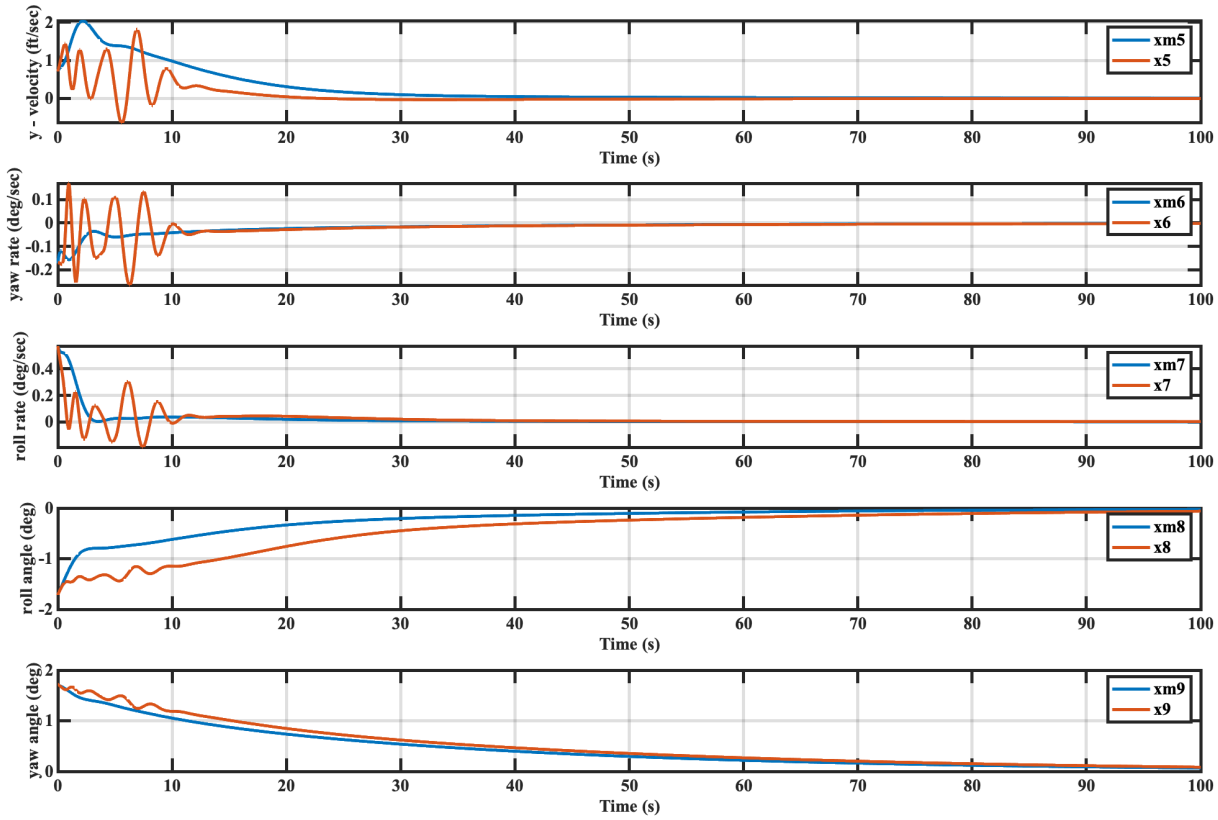

Figure 5-8. System states $x_5 = v$, $x_6 = r$, $x_7 = p$, $x_8 = \phi$, $x_9 = \psi$ (Case IV)

5.6 Case VI

Case VI demonstrates what happens when increased learning rates and adaptive gains cause control saturation. The system experiences an instantaneous rudder failure and right aileron failure. In this case $\Gamma = .005 \times I_{9x9}$ and $\lambda = [.01\ .05\ .05\ .02\ .02\ .02]$. The results are shown in Figures 5-11 and 5-12.

Both figures show an amplified version of the negative effects shown in Cases IV and V. This learning rate is now moving too quickly for the control surface rate and deflection limits to handle. This causes highly undesirable flight characteristics to arise in the state outputs.

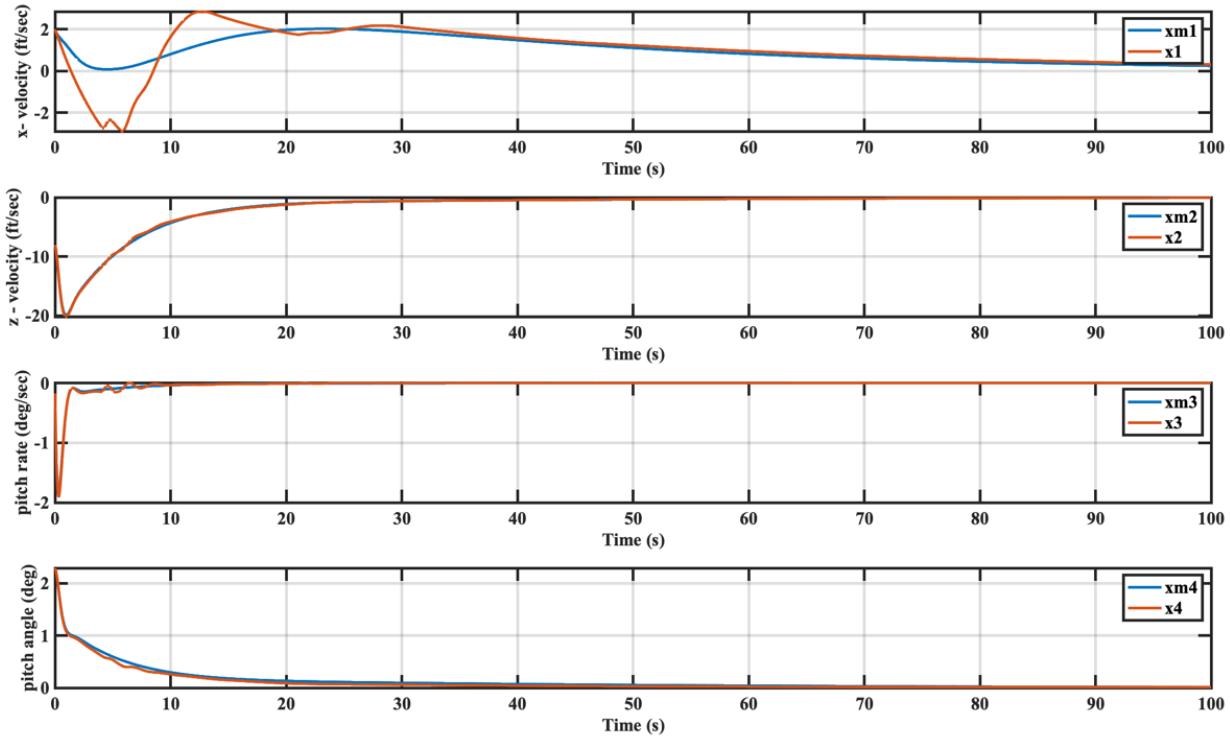

Figure 5-9. System states (top to bottom) $x_1 = u$, $x_2 = w$, $x_3 = q$, $x_4 = \theta$ (Case V)

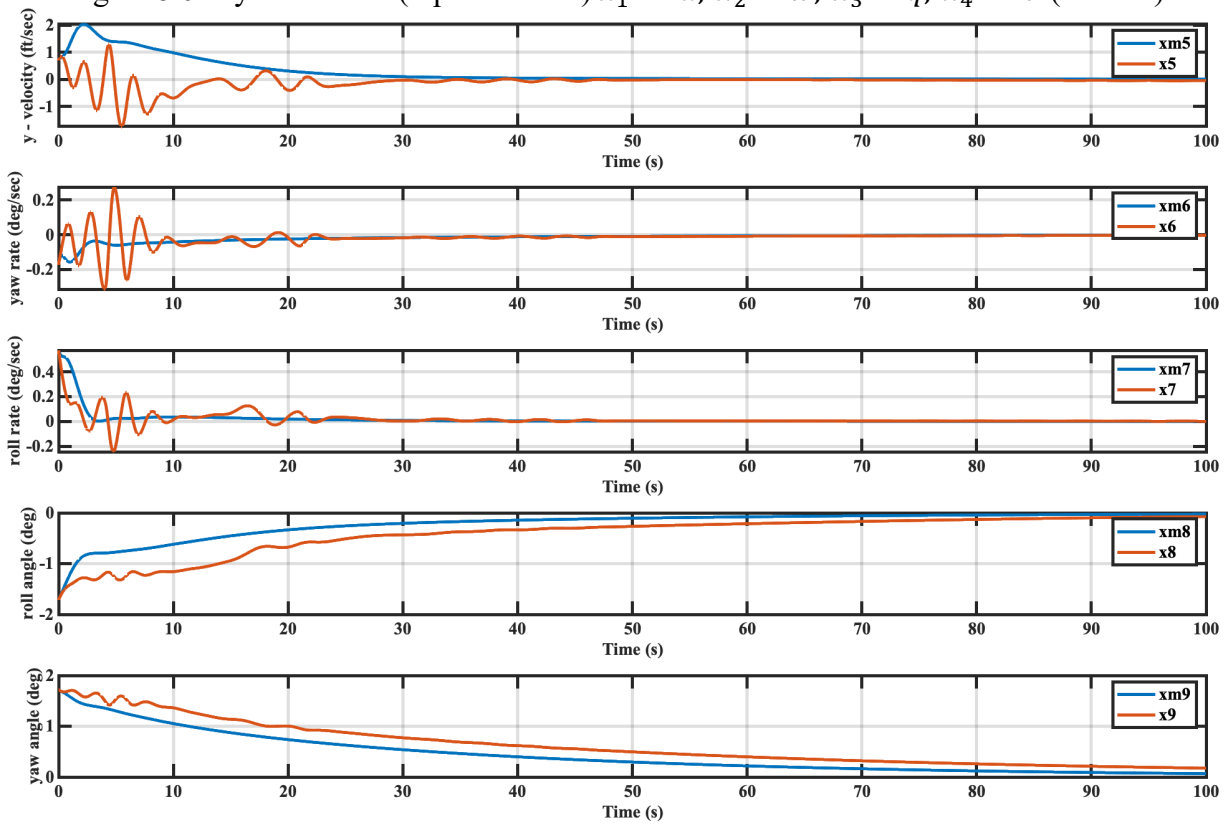

Figure 5-10. System states $x_5 = v$, $x_6 = r$, $x_7 = p$, $x_8 = \phi$, $x_9 = \psi$ (Case V)

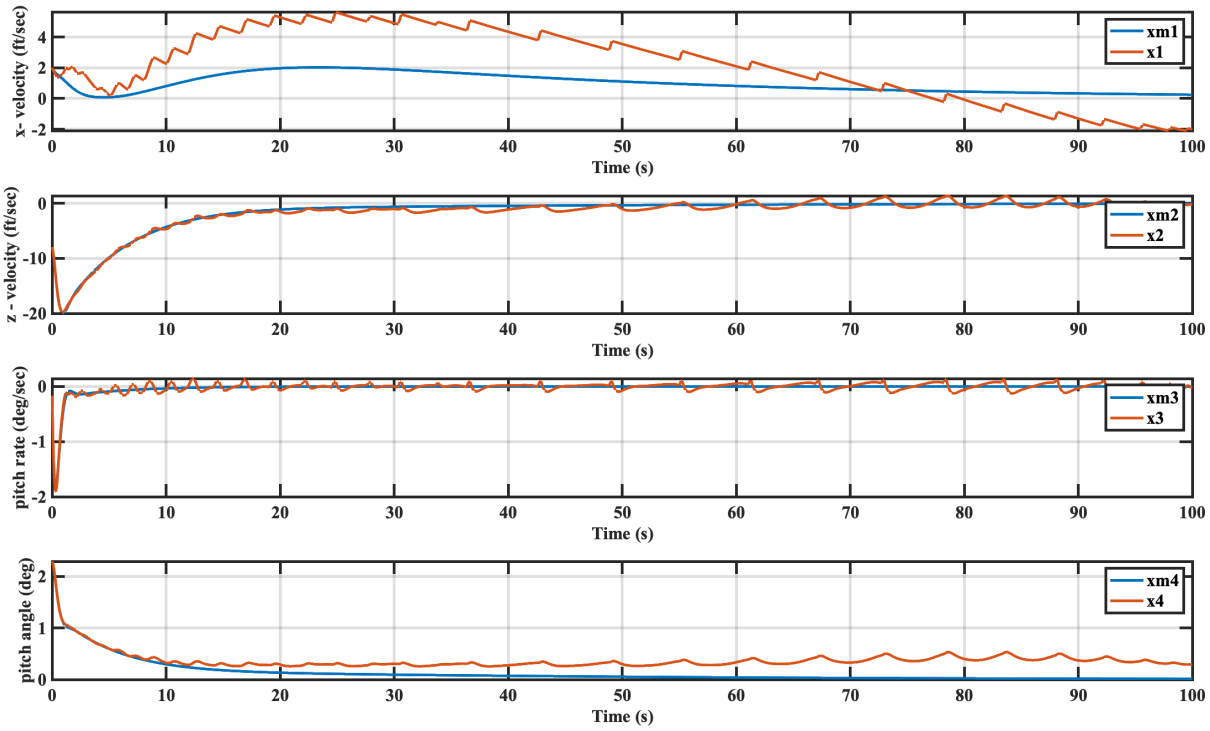

Figure 5-11. System states (top to bottom) $x_1 = u$, $x_2 = w$, $x_3 = q$, $x_4 = \theta$ (Case VI)

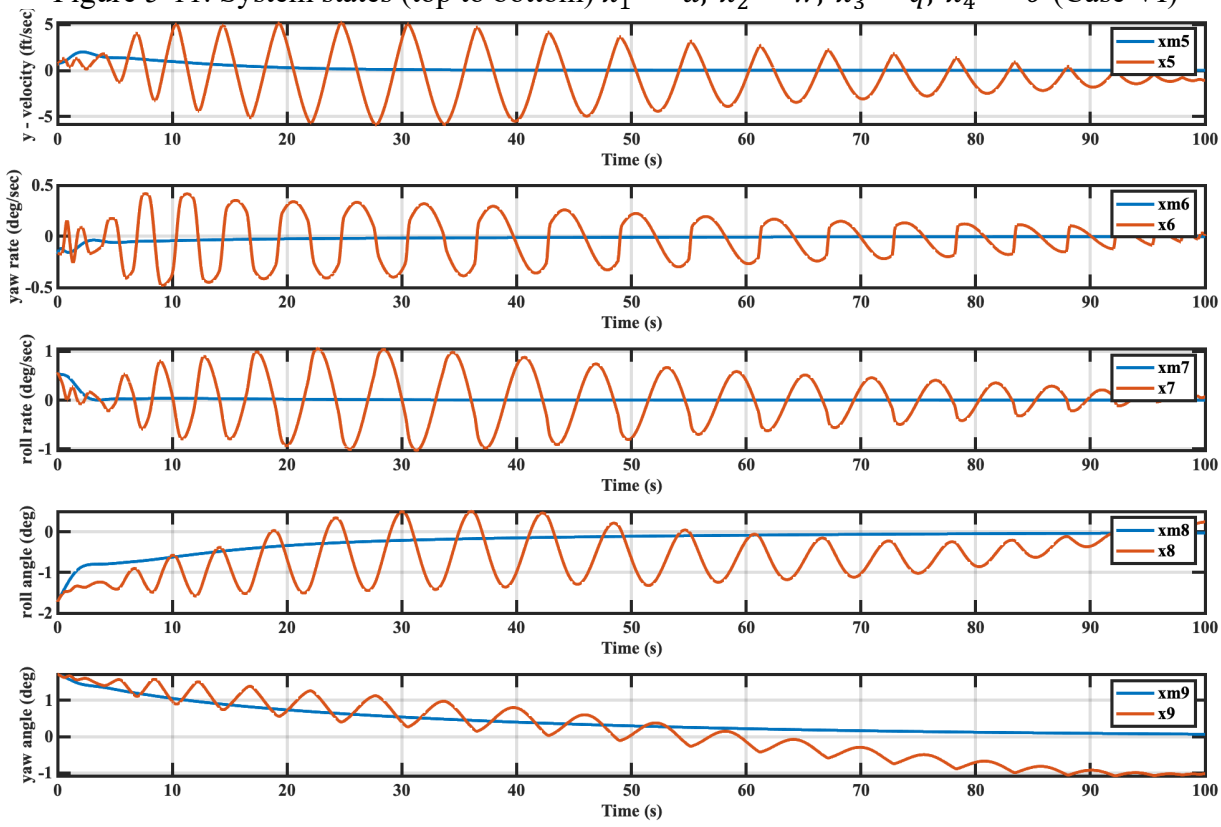

Figure 5-12. System states $x_5 = v$, $x_6 = r$, $x_7 = p$, $x_8 = \phi$, $x_9 = \psi$ (Case VI)

Chapter 6

Conclusion

This thesis aimed to prove the viability of adaptive control surface failure compensation in transport type aircraft. A differential thrust aircraft model was developed and linearized with respect to a wings level unaccelerated flight condition. The model's features were independent engine and aileron operation in addition to the coupling of the lateral and longitudinal flight dynamics. This allowed the coupled dynamics to be studies over a range of actuator failures.

After the model was developed a nominal LQR controller was implemented and tuned using real world flight dynamics considerations. This controller was integrated with a linearized plant model to form the model reference for the adaptive mechanism. The adaptive controller consisted of the model reference and the implementation of two adaptive laws described in Chapter 3. Together these elements were integrated with the aircraft plant in a MATLAB and Simulink simulation.

A small subset of possible failure patterns were presented in this paper. The failure patterns discussed included rudder, aileron, and thrust failures which yielded mostly lateral control difficulties. Another important aspect discussed in this paper was the role of control saturation when using adaptive control. This element was not studied in any of the reference material.

The results of all simulations yielded useful conclusions. Similar results to [2] are duplicated and verified here. Engine thrusts can adequately and effectively compensate for rudder and aileron failures. Rudder and aileron inputs are the primary control surfaces used by pilots and conventional flight controllers for lateral control and stability. The integration of engine thrusts as a secondary lateral controller shows significant promise. The results of the reference material are further

validated with the addition of control surface rate and deflection limits. With the appropriate adaptive gains, the adaptive controller shows asymptotic convergence to the reference model without saturating the controls. It does so with a healthy margin for error.

Additionally, engine failures are evaluated for response by the adaptive controller. Engine failures are some of the most critical emergencies aircraft pilots face. It often completely removes the ability to use automatic flight control. The adaptive controller was able to compensate for these failures successfully and well within tolerances for stable flight. These results were also accomplished without control saturation.

Finally, the results also evaluated a threshold for learning rates by showing when an increase in rate will result in control saturation and system instability. This opens the door for an entire subset of evaluation when designing aircraft to be flown by automated adaptive controllers. Properly designing certain control surfaces to move quicker and with a larger range can enable the aircraft to deal more effectively with a wide range of failure patterns.

The adaptive control scheme was able to return the aircraft to the trim flight condition from its perturbed initial state in all failure patterns evaluated in this paper. As previously mentioned, most of these failure patterns provided a lateral control problem. Further study will show system responses to longitudinal control problems as well. As shown is section 1.9 the lateral system is the most subject to inherent instability. Therefore, showing successful system performance with lateral control failures bodes well for the success of the controller over all recoverable failure patterns.

The study of reference tracking with this same controller should also be evaluated in further study. This thesis only evaluated the return to a trimmed flight condition rather than the reference tracking needed to pilot the degraded aircraft. Upon initial inspection this controller successfully accomplished reference tracking as well however, further evaluation with a nonlinear plant and time varying environmental conditions is needed.

This line of research has the potential to launch a new generation of aircraft and spacecraft controllers. Proving convergence mathematically and in simulation will only partially drive implementation in production vehicles. The road to building trust with pilots and aircrew involves an impeccable record of performance in test vehicles over a wide range of operating conditions.

Bibliography

[1] F. W. Burcham, J. J. Burken, T. A. Maine, and C. G. Fullerton, "Development and Flight Test of an Emergency Flight Control System Using Only Engine Thrust on an MD-11 Transport Airplane," 1997.

[2] Y. Liu, X. Tang, G. Tao, and S. M. Joshi, "Adaptive Failure Compensation for Aircraft Flight Control Using Engine Differentials: Regulation."

[3] Y. Liu, X. Tang, G. Tao, and S. M. Joshi, "Adaptive failure compensation for aircraft tracking control using engine differential based model," in *Proceedings of the American Control Conference*, 2006, vol. 2006, pp. 5984–5989. doi: 10.1109/acc.2006.1657680.

[4] T. I. Fossen, "MATHEMATICAL MODELS FOR CONTROL OF AIRCRAFT AND SATELLITES 3rd edition," 2013.

[5] B. L. Stevens, F. L. Lewis, and E. N. Johnson, *Aircraft Control and Simulation: Dynamics, Controls Design, and Autonomous Systems*. Hoboken, NJ, USA: John Wiley & Sons, Inc, 2015. doi: 10.1002/9781119174882.

[6] Jeffrey B. Burl, *Linear Optimal Control*, 1st ed. Menlo Park: Addison Wesley Longman, Inc., 1998.

[7] J.-J. Slotine and W. Li, *Applied Nonlinear Control*.

[8] Y. Liu and L. G. Crespo, "Adaptive control allocation in the presence of actuator failures," *Journal of Control Science and Engineering*, vol. 2012, 2012, doi: 10.1155/2012/502149.

[9] F. W. Burcham, J. J. Burken, T. A. Maine, and C. G. Fullerton, "Development and Flight Test of an Emergency Flight Control System Using Only Engine Thrust on an MD-11 Transport Airplane," 1997.